Mathematical human body modeling in impact shoulder and upper extremity

Bours, R.C.H.

Award date:
2000

Mathematical Human Body Modeling in Impact

- Shoulder and Upper extremity -

WFW-report 2000.013

R.C.H. Bours

Master's Thesis, May 2000

Examination-board:

Prof. Dr. Ir. D.H. van Campen	(TUE)
Prof. Dr. Ir. J.S.H.M. Wismans	(TNO/TUE)
Dr. Dr. P.H.M. Bovendeerd	(TUE)
Dr. Ir. R. Happee	(TNO/TUE)
Dr. H.E.J. Veeger	(VU/TUD)

Eindhoven University of Technology
Faculty of Mechanical Engineering
Eindhoven, The Netherlands

TNO Automotive
Crash Safety Centre
Delft, The Netherlands

To whom shall I give it, my new little book
All polished with pumice and daintily dight?
Cornelius, take it! For ever you look
At my trifles with favour, expressing delight.

Alone of Italians you ventured to tell
The tale of the ages - three volumes, they say,
And, by Jupiter, learned and written full well,
And compiled with due care in a scholarly way.

So take, friend of mine, this pretence of a book,
Be it worthy or not of the ink on the page
Yet, 0 Muse, 'tis with favour I pray you may look,
That it linger unfading for more than an age.

Gaius Valerius Catullus (84-54 BC)

Summary

The introduction of seat belts and airbags in vehicles has reduced the incidence of fatal traffic accidents, but they have increased the risk of non-fatal injuries including those to the shoulder and upper extremity. Because of the high social and medical costs associated with these injuries, it is important to understand the mechanisms of these injuries and to develop injury reduction measures.

The main objective of this study is the development of a design and research tool to evaluate shoulder and upper extremity interaction with airbags, car interiors and seat belts. Literature study showed that existing shoulder models were mainly lacking a biofidelic input resulting in poor validation results, and hence poor injury prediction capabilities. Therefore, it was decided to develop an improved shoulder and upper extremity model.

A multibody shoulder and upper extremity model is proposed consisting of rigid bodies for the clavicle, scapula, upper arm, lower arm and hand, which are connected by kinematical joints and force models. The geometrical, inertial and biomechanical properties are based on experimental data found in literature. The joint characteristics are based on volunteer experiments performed by Engin. Deformation properties of the clavicle are derived from axial compression experiments performed at the University of Heidelberg. Because of limitations of the thorax model algorithm, it was not possible to connect the shoulder model to the thorax model and therefore, the shoulder model is connected directly to the spine. Though, thorax deformation characteristics are included and based on simulations with a finite element thorax model developed at TNO Automotive.

Lateral evaluation of the shoulder model is performed using PMHS lateral pendulum tests and PMHS lateral sled tests. Acceptable correlation between the model response and the experimental data is achieved. The model is capable of predicting the load transfer from shoulder to spine through different loadpaths and it predicts well deformations occurring in the shoulder girdle. Due to a lack of experimental data no quantitative conclusions are drawn about other directional responses. Evaluation of the multibody upper extremity model is performed with a limited amount of data, and showed that available experimental data are not sufficient. Compared to existing models, the multibody shoulder and upper extremity model show major improvements in the field of realistic input, biofidelic response and injury prediction capability.

Also, a finite element clavicle model is developed and integrated with TNO's finite element thorax model and TNO's multibody human model. Comparison of the response of this finite element/ multibody model and the complete multibody model showed the necessity of a biofidelic shoulder - thorax interaction.

Contents

Chapter 1

Introduction

This report deals with the work of a master's project, which is part of a co-operation between the Technical University of Eindhoven, Faculty of Mechanical Engineering and TNO Automotive, Crash Safety Centre. The work contributes to the development of a 50^{th} percentile male human body model at TNO Automotive. TNO's objective is to build numerical models of the human body, which are based on an accurate definition of the human anatomical geometry and biomaterial properties.

1.1 Context of this study

The number of traffic deaths in the Netherlands has decreased since 1972. In 1998, the number of traffic deaths was at a same level as in The Fifties. This is remarkable considering the increase of road vehicles during this same period [1]. This remarkable decrease can be ascribed to successful fatality reduction strategies, which resulted in improved vehicle safety. In order to determine the effectiveness of safety measures in motor vehicles, a lot of attention has been given to the development of mechanical models of the human body: The crash test dummies. These substitutes have similar response characteristics as human beings and, being fitted with special instrumentation, they enable injuries to be assessed. In order to optimize design processes, mathematical models of crash test dummies are widely used. However, these models inherit the same discrepancies as exist between dummies and the real human body.

An increasing consciousness in auto-industry to improve occupant safety for a wider range of crash situations than covered by current regulations, demands more advanced tools, such as human body models. Among these mathematical human models, research is mainly focused on the vulnerable body parts, like the thorax and neck region. The resulting safety measures have reduced the risk of fatal injuries, but they have increased the relative incidence of non-fatal injuries including those to the shoulder and upper extremity.

For instance airbags have contributed to a reduction of thorax injury in frontal impact. However, when car occupants sit abnormally close to the airbag, the airbag can induce bone fracture and joint injury to the upper extremity during deployment. This problem is generally referred to as *out of position* (OOP) airbag interaction. Recently side-airbags

have been introduced as well. The design space is limited and therefore side airbags easily provide some sort of OOP interaction. Side airbags are suspected to cause injuries to shoulder and upper extremity, but due to their recent introduction such effects are not yet seen in accident databases.

It has been recognized that the biomechanical response of the upper extremity has a major influence on the protection of vital areas. In frontal impact the shoulder interacts with belt systems and airbags. It is essential that belt systems are designed such that belts do not slip off the shoulder. In side impact the shoulder interacts with vehicle interior and airbags.

1.2 Objectives

The main objective of this study is the development of a mathematical model - as design and research tool - to evaluate shoulder and upper extremity interaction with frontal airbags, side airbags, car interiors and belts. The model needs to have injury prediction capability for: (i) fractures of clavicle, humerus, ulna and radius; (ii) dislocation of shoulder joints; and (iii) injury to the elbow and wrist joint. The shoulder and arm model described in this report is a first step in the development of this injury prediction tool. The following objectives are stated:

- The model has to be able to simulate global biofidelic kinematics of a 50^{th} percentile male shoulder/upper extremity during impact conditions. The model has to predict the global response of the shoulder girdle during lateral, frontal and upward loading. This response can be evaluated with the results of pendulum impacts in frontal and lateral direction, and whole body sled tests in lateral and frontal direction with/without airbags and/or belts.

- The model has to be able to provide the transfer of forces from the arms to the thorax through different load paths. A realistic interaction between the shoulder complex and the thorax is necessary to predict the transfer of forces from the arm to the thorax/spine. The load transfer from shoulder to spine is possible through the skeletal connection (humerus - scapula - clavicle - sternum - ribs - spine) and through the thoraco-scapular sliding connection (humerus - scapula - ribs - spine). A realistic description of the thoraco-scapular connection will result in a biofidelic load transfer and improved shoulder kinematics.

- Prediction of deformation and failure of the separate body structures during different loading conditions is needed in order to provide a biofidelic interaction with belts, frontal/side airbags and internal car structures. Deformation and failure behavior can be studied with the results of mechanical tests on isolated clavicles, scapulae and arm bones.

- The model should predict a realistic relative movement of body segments connected by joints in order to predict dislocations of shoulder joints. Dislocations are a result of ligament/muscle rupture due to extreme rotations and/or translations. Detailed modeling of ligament and muscle structures is not within the scope of this study

- A better understanding of the impact mechanics of the shoulder will be gained with the kinematic (displacements, velocities, accelerations and forces) and mechanical (stresses and strains) response information. This information will be used to develop kinematical and mechanical injury criteria for shoulder and upper extremity.
- Preferably, the model also has to simulate injury mechanisms. In this way, the model represents the kinematics and mechanics of a person who sustained fractures and thereby represents the altered behavior caused by these fractures.

Since the shoulder and upper extremity models have to predict the response of car occupants during traffic accidents, resulting in dynamic impact conditions, the models do not necessarily have to predict the response to (quasi-)static loading conditions.

1.3 Outline

One of the first criteria for a biofidelic shoulder/ upper extremity model is the implementation of realistic geometrical and biomechanical data. A literature review on the anatomical description of the shoulder and arm and biomechanical data is presented in Chapter 2. In order to get information about the feasibility of the objectives stated in Section 1.2, results of a bibliographic study on experimental data are presented in Chapter 3. A large number of models describing the shoulder mechanism have been published, but only a few describe the response in impact conditions. The most recent and relevant models will be discussed in Chapter 4. In Chapter 5 a description and explanation of the multibody shoulder and upper extremity model set-up is given. Validation of these models is given in Chapter 6. Finite element techniques are applied to get better understanding of the deformations occurring in different components of the shoulder. These models and the results are discussed in Chapter 7. This is followed by a discussion, conclusions and recommendations for future research.

Chapter 2

Anatomy and biomechanics

Biofidelic shoulder and upper extremity modeling needs understanding of the functional anatomy and biomechanical behavior of the human shoulder and arm. A bibliographic study on the anatomical description of the shoulder and arm and biomechanical data is presented in Section 2.1 and 2.2.

2.1 Functional anatomy

2.1.1 The human shoulder

The shoulder mechanism forms a moving base for the upper extremity. It contains a number of joints connecting the humerus, the scapula, the clavicle and the sternum. Furthermore, the scapula contacts the posterior side of the thorax. This connection makes the shoulder complex a closed-chain mechanism. The term 'shoulder complex' refers to the combination of the shoulder joint (the glenohumeral joint) and the shoulder girdle, which includes clavicle and scapula and their articulations. Anterior and posterior views of the overall skeletal structure of the human thorax, shoulder girdle and arm are illustrated in Figures 2.1(a) and 2.1(b). A brief overview of anatomical terminologies used in this report is given in Appendix A.

Position changes of the arm involve movements of the clavicle, scapula and humerus. These movements are the result of the combined work of the sternoclavicular, acromioclavicular and glenohumeral joints, and the scapulothoracic gliding mechanisms [3, 4, 5].

The *sternoclavicular* joint (shown in Figure 2.2(a)) is a plane synovial articulation in which the bulbous medial end of the clavicle articulates with a shallow sternal socket and with the cartilage of the first rib. Anterior and posterior sternoclavicular ligaments reinforce the capsule and limit anterior-posterior movement of the medial end of the clavicle. The costoclavicular ligament attaches the inferior surface of the medial end of the clavicle to the first rib. It acts as a check to clavicular elevation and helps limit clavicular protraction. Although the articular surfaces of the sternoclavicular joint are saddle-shaped, the joint functions as a ball-and-socket joint, with three degrees of freedom.

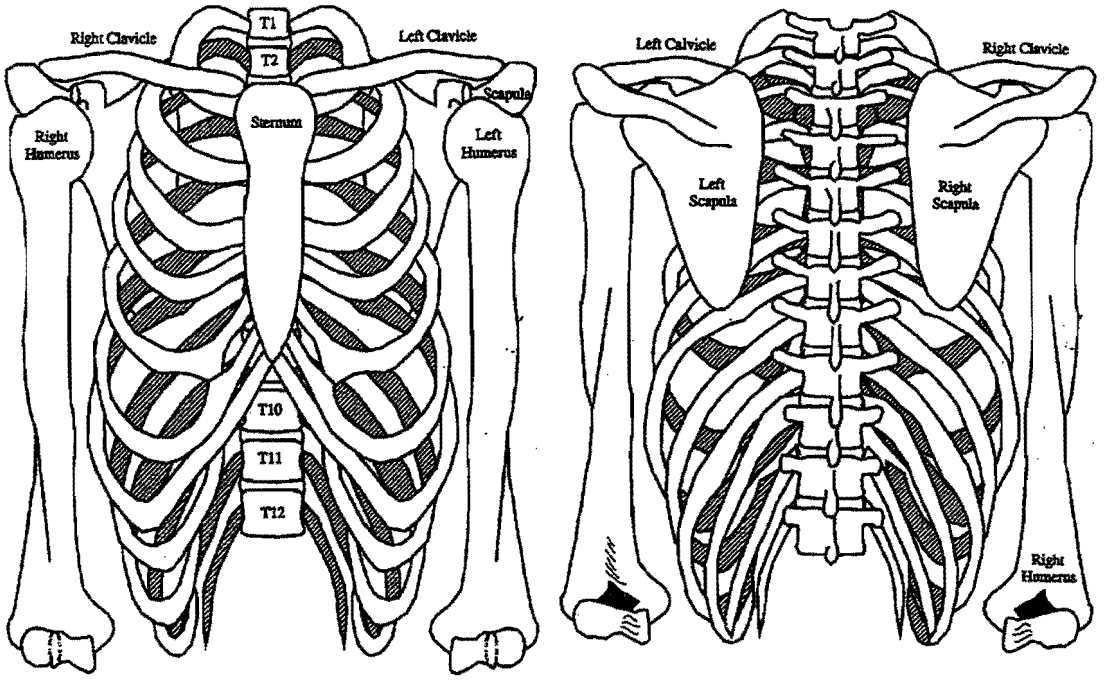

(a) Anterior (b) Posterior

Figure 2.1: Anterior and posterior skeletal view of the human thorax, shoulder and arms [2].

The *acromioclavicular* joint (shown in Figure 2.2(b)) is also a plane synovial joint between a small convex facet on the lateral end of the clavicle and a small concave facet on the acromion of the scapula. Stability of the acromioclavicular joint is dependent on the superior and inferior acromioclavicular ligaments that reinforce the weak joint capsule. In addition, the strong coracoclavicular ligament, uniting the clavicle and the coracoid process of the scapula, is important in maintaining the relationship of the two bones. The acromioclavicular joint allows movement of the acromion, and thus the scapula, on the lateral end of the clavicle. The joint is important because it contributes to total arm movement in addition to transmitting forces between the clavicle and the acromion. Functionally, the two major movements at the acromioclavicular joint are a gliding movement as the shoulder joint flexes and extends, and an elevation and depression movement to conform with changes in the relationship between scapula and the humerus during abduction.

The *glenohumeral* joint is a synovial ball-and-socket joint between the humeral head and the glenoid fossa of the scapula. Because the head of the humerus is larger than the glenoid fossa, only part of the humeral head can be in articulation with the glenoid fossa in any position of the joint. Since passive structures in and around the glenohumeral joint do not guarantee joint stability, the glenohumeral joint has to be actively stabilized [6, 7]. This stabilizing function is generally attributed to a group of four muscles, called

the rotator cuff.

Except for attachments through the acromioclavicular and sternoclavicular joints, the scapula is without bony or ligamentous attachments to the thorax. The *scapulothoracic* gliding mechanism is not a true joint but is the sliding of the concave anterior surface of the scapula on the convex posterior-lateral surface of the thoracic rib cage. The thorax and scapula are separated by two muscles, which glide over each other during movements of the scapula. The scapula is held in close approximation to the thorax wall by muscular attachments. In movements of the shoulder complex, the scapula can be protracted, retracted, elevated, depressed, and rotated about a variable axis perpendicular to its flat surface.

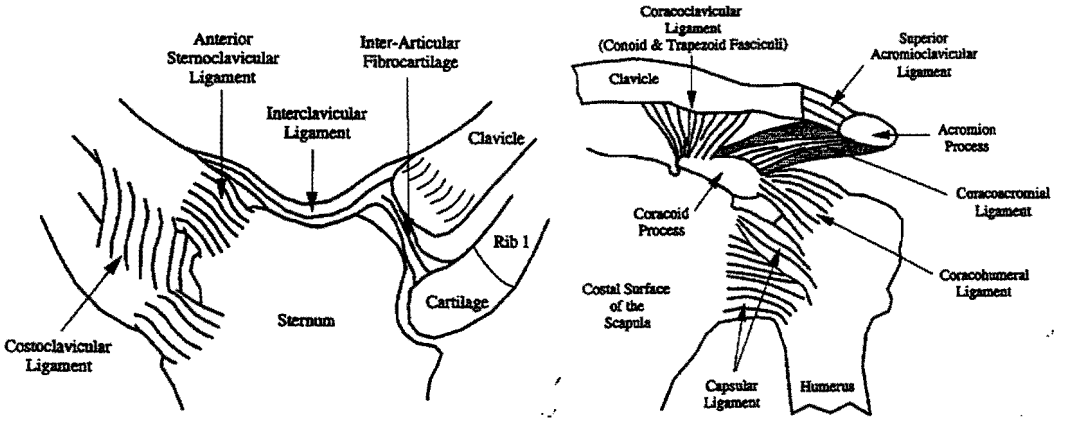

(a) Sternoclavicular joint (b) Acromioclavicular joint

Figure 2.2: Anterior views of the sternoclavicular joint and acromioclavicular joint [2].

2.1.2 The human upper extremity

The upper extremity is composed of five morphologically distinct regions: The upper arm (humerus and tissues), elbow, lower arm (ulna, radius and tissues), wrist and hand. The distal head of the humerus and the proximal ends of the radius and ulna comprise the elbow joint (see Figure 2.3). Flexion/extension of the elbow joint is guided by the throchlear notch of the ulna which rotates along the throchlea of the humerus. Additionally, the proximal radius head rotates on the capitulum of the distal humerus (the superior radio-ulnar joint) to allow for the elbow contribution of the pronation/supination movement. This movement is completed by the ulna rotating at the wrist (inferior radio-ulnar joint). This inferior joint is anatomically separate from the wrist. In supination the radius and ulna lie side by side with the ulna on the medial side; their axes are parallel. In pronation these bones are no longer parallel, but cross each other; the radius is lateral to the proximal end of the ulna and medial to it distally. The wrist contains two joints: (1) the radio-carpal joint between the radial head and the proximal row of carpal

bones; (2) the mid-carpal joint between the proximal and distal rows of carpal bones. The wrist joint allows for two motions: flexion/extension and abduction/adduction.

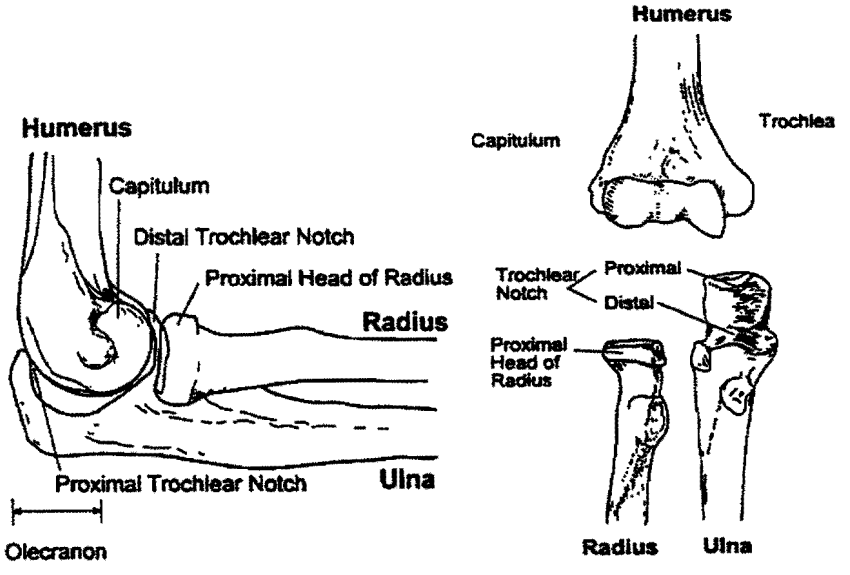

(a) Lateral view (b) Frontal view

Figure 2.3: Lateral and frontal view of the elbow joint [8].

2.2 Biomechanics

The effectiveness of a mathematical model to predict accurately live human response depends heavily on the proper biomechanical description and simulation of the articulating joints. Short time response of a multi-segmented model requires proper characterization of the motion range, the passive resistive force, moment and damping properties data in articulating joints. The research and studies on the shoulder complex has more than a century long history, and a brief summary of the subject manner prior to 1980 is provided by Engin [9]. Biomechanical models of the human shoulder complex range from a qualitative planar kinematical model [10] to quasi-static [11, 12] and dynamical, musculoskeletal models [7]. The success of biomechanical modeling of the shoulder complex is generally hindered by the lack of appropriate data as well as the anatomical complexity of the region. Engin and Chen [13] have established a statistical *in-vivo* data base for the shoulder complex sinus. A joint sinus is the total range of angular motion permitted by a moving link of a joint with respect to the other rigidly fixed link. They expressed the numerical results in functional expansion form relative to a locally defined joint axis system. Engin and Chen [14, 15] have determined the three-dimensional passive resistive joint properties beyond the maximal voluntary shoulder complex sinus. Engin and Tümer [16] proposed a three-dimensional kinematic model by utilizing the concepts of

kinematic links, joints and joint sinuses. The statistical *in-vivo* data base, reported by Engin and Chen, is cast in a form compatible with their model by obtaining a set of unit vectors describing circumductory motion in a torso-fixed coordinate system. They give numerical results for angles and orientations of the composite joint sinus cone, between thorax and humerus, with respect to the anatomical directions. Tümer and Engin [17] have determined individual joint sinuses associated with the sternoclavicular, acromioclavicular and glenohumeral joints. They employed the statistical *in-vivo* data base for the circumductory motion of the upper arm to determine a set of joint variables via optimization, which are then utilized to establish the sizes and orientations of the elliptical cones for the individual joint sinuses. Since the range of motion of the humerus axial rotation was not reported by Engin and Tümer, Wang and coworkers [18] extended the shoulder kinematic database established by Engin and Tümer with the quantification of the motion range of the humerus rotation along the longitudinal axis.

Joint motion ranges

The excursions of the separate segments of the shoulder and arm are limited by the mobility ranges of their joints. These limitations result from stretching the joint ligaments into taut states and from bone to bone contact. In Table 2.1 reported data on the motion range of the sternoclavicular, acromioclavicular, glenohumeral, elbow and wrist joints are presented.

Dempster [19] has collected a limited amount of data on specially prepared cadaveric specimens. Engin and Tümer obtained data by employing an optimization criterion [17] on the statistical database for the humerus orientation during circumductory motion of the arm. The data show a good agreement between the theoretical results of Engin and Tümer and the measurements on cadaveric specimens by Dempster. However, one should note that the theoretical values are based on *in-vivo* data base, whereas the ones obtained in *in-vitro* experiments did not include muscle actions. In both their work, the upper arm axial motion range was supposed to be independent of the position of the upper arm in the shoulder joint sinus cone and the axial motion range of the clavicula, scapula and humerus are not reported. Wang *et al.* [18] reported an extension of the results by Engin and co-workers. They measured the motion range of the upper arm rotation along the longitudinal axis with respect to the thorax. It was shown that the upper arm motion range depends strongly on the position of the upper arm. Furthermore, motion ranges for the sternoclavicular and 'composite' motion ranges for the acromioclavicular/glenohumeral joint are provided by the RAMSIS software package [20]. Kapandji summarizes motion ranges for all joints in the human shoulder and arm complex, but does not provide the sources for these data [21].

Passive resistive properties

As mentioned earlier, Engin and Chen [13, 14] were the first to provide statistically meaningful *in-vivo* data for the kinematics of the shoulder complex. Their data collection methodology [22], which utilizes sonic emitters and data analysis technique based

on selection of the 'most accurate' data set, has also been applied to provide passive resistive properties of the human shoulder complex [23, 24]. They have provided a method for obtaining restoring force data for forced excursions of the upper arm beyond its voluntary motion range and presented passive restoring forces versus angular displacement for different postures of the arm. The maximum restoring force value obtained in each test was dependent on either discomfort experienced by the subject or interference with another body segment. They concluded that the constant restoring forces are not simply an outward expanded version of the maximal voluntary joint sinus. They also showed that the shoulder is less 'stiff' for angular displacements in the rear 'quadrants' (20-40 Nm/rad.) than in the front 'quadrants' (40-70 Nm/rad.).

Source	**Motion range [°]**				
	SC joint	AC joint	GH joint	Elbow	Wrist
	abduction/adduction				
Dempster	35	30	100	-	-
Engin/Wang	28	28	95	-	-
Ramsis	40	160			
Kapandji	210			0	60
	axial rotation			pro-/supination	
Dempster	-	30	-	-	-
Engin/Wang	94 - 157			-	-
Ramsis	20	170			
Kapandji	30	30	-	185	0
	flexion/extension				
Dempster	44	60	160	-	-
Engin/Wang	46	39	135	-	-
Ramsis	50	215			
Kapandji	230			150	170

Table 2.1: Average motion range of the joints of the shoulder complex and upper extremity based on Dempster[19], Engin and Tümer[17], RAMSIS[20] and Kapandji[21]

Damping properties

Determination of the damping properties in articulating joints is an important part of proper biomechanical description. Engin [25] presented a simple and reliable method for experimental determination of the angular damping coefficients of articulating joints. They presented the calculated angular damping coefficients for forty different orientations of the arm with respect to the torso. Nothing is mentioned about rotational velocities during the experiments. The angular damping coefficients were in the range 0.30 - 0.60 Nms/rad.

Chapter 3

Response Requirements

The shoulder and arm model are evaluated by comparing its response to experiments found in literature. Globally, three kind of tests can be distinguished: (i) PMHS (Post Mortem Human Subject) impactor tests, (ii) PMHS sled tests, and (iii) mechanical tests on body components. These tests are described in the following sections after an introduction about normalization of test results.

3.1 Normalization

The physical dimensions of the cadavers, used in experiments, vary considerably from those of a 50^{th} percentile male. Consequently, the measured forces, accelerations and displacements of these subjects are expected to be different from those obtained if a 50^{th} percentile male cadaver had been subjected to the same test conditions. Normalization is a technique used to estimate the response of a 50^{th} percentile male from the responses of different sizes of subjects. The normalization procedure proposed by Mertz [26] and used by the International Standards Organization was applied to the experimental data described in this chapter. Mertz used a simple mass and spring model to demonstrate that both the effective mass involved in the impact and the effective spring constant need to be considered when normalizing impact response data. This method does not take into account the variability of individual cadaver characteristics as bone condition, age and shape. Also, viscoelastic effects are not included.

3.2 Lateral impactor tests

APR

Researchers of the Association Peugeot-Renault subjected four cadavers to lateral impacts applied by the flat end of a 23.4 kg rigid cylinder [27]. The cylinder (150mm diameter) impacted the shoulder at a velocity of 4.5m/s. Each cadaver was seated on a horizontal surface with a vertical backrest. The hands were placed on the lap and the impacted arm was suspended as if supported by an armrest. The model of the set-up is

shown in Figure 3.1. The force and acceleration of the impactor, the acceleration of the thoracic spine, and the deflection of the shoulder relative to the thoracic spine were measured. The impact data were normalized to represent the response of a 50^{th} percentile adult male by means of the normalization technique of Mertz [26]. Only three of the four APR tests have been used by the International Organization for Standardization [28] to derive biofidelity response requirements, since one of the tests yielded a different shaped response and an impulse inconsistent with the other three. Full details on the test procedures and results from these tests have not been widely published. The experiments resulted in force versus time and maximum shoulder deflection response requirements. The ISO shoulder biofidelity corridors are presented in Table 3.1. They proposed a range for the maximum shoulder to thoracic spine lateral deflection of 37.5±3.5 mm.

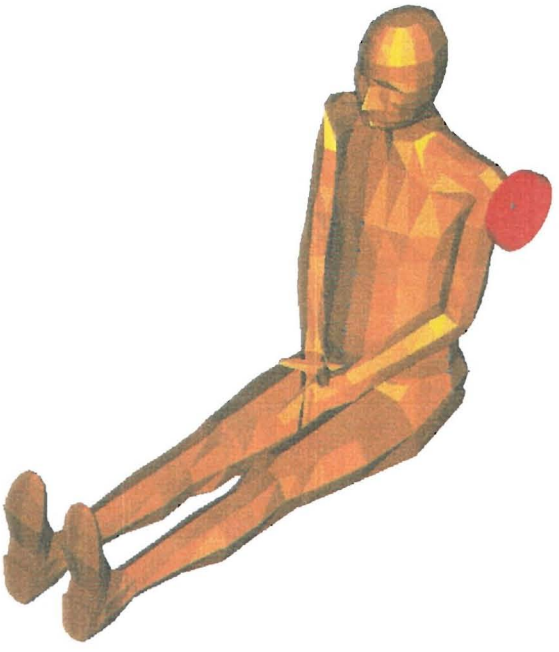

Figure 3.1: Model set-up of the APR pendulum impact.

LBA

Meyer of the Laboratory of Applied Biomechanics, Marseille applied lateral impacts at seven cadavers with a 23.4 kg rigid, square guided impactor. The square impactor (100mm x 100mm) impacted the shoulder (on the head of the humerus) at a velocity of 5.5m/s. The experiments resulted in force versus time response requirements, which are presented in Table 3.2.

Time [ms]	Lower limit [kN]	Upper limit [kN]
0.0	0.0	1.6
6.0	-	2.8
13	1.7	-
26	-	2.8
42	0.6	-
57	-	1.0

Table 3.1: ISO Force - Time response requirements for lateral shoulder impactor tests

Time [ms]	Lower limit [kN]	Upper limit [kN]
0.0	0.0	0.0
2.0	-	4.1
8.0	2.6	-
18.0	0.0	-
20.0	-	3.5
32.0	-	1.2
50.0	-	0.5

Table 3.2: LBA Force - Time response requirements for lateral shoulder impactor tests

3.3 Lateral sled impact

WSU

A series of rigid wall lateral impacts has been conducted by researchers of Wayne State University. Cavanaugh [29] described the test conditions in detail and Irwin *et al.* [30] analyzed the data. Only two out of seventeen subjects were used in rigid wall impacts. SIC04 (Side Impact Cadaver) struck the flat, rigid impact surfaces at a speed of 9.1m/s; SIC07 at a speed of 6.7m/s.

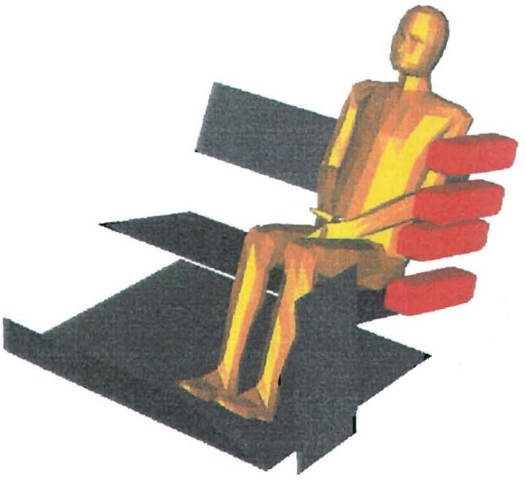

Figure 3.2: Model set-up of the WSU lateral sled impact.

The tests were conducted on a Heidelberg-type sled apparatus: The test subjects were placed in a seated position at the rear end of a bench seat. At the front end of the bench seat an instrumented, rigid wall was placed to stop the test subject and to measure the impact at the level of the shoulder, thorax, abdomen, pelvis and knee. Rapid decelera-

tions of the sled caused the cadaver to slide along the flat, smooth seat before impacting the rigid wall. The cadaver's arms were positioned 15° forward of the longitudinal axis. The wrists were taped together and rested on the lap. The model of the set-up is shown in Figure 3.2. In addition to the instrumentation of the rigid wall with nine load cells, the cadaver was instrumented with head, chest, and spinal accelerometers. Photo targets were attached on thoracic vertebrae T1 and T5, the upper and lower sternum, the spinous process of the left scapula, the medial and lateral ends of the left clavicle, and non-impacted acromion to measure regional deformation for impact with the rigid wall. Table 3.3 summarizes anthropometric information and the skeletal injuries to the thorax and shoulder of both rigid impact cadavers.

Subject	**Age** (years)	**Sex**	**Mass** (kg)	**Shoulder injury**	**Thorax injury**
SIC 04 ($9.1m/s$)	69	Male	57.6	Left acromion separation Left acromion fracture	19 left rib fractures 3 right rib fractures
SIC 07 ($6.7m/s$)	66	Male	74.8	Left acromion separation Left acromion fracture	13 left rib fractures 3 right rib fractures

Table 3.3: Cadaver properties and observed injuries of the shoulder and thorax

The following useful results were obtained from the rigid wall impacts to evaluate the shoulder model: Displacement of the non-impacted acromion, displacement and acceleration of the first thoracic vertebra T1, displacement of the fifth thoracic vertebra T5, displacement of the lower sternum, accelerations of the impacted shoulder and contact forces between shoulder/thorax and the rigid wall.

NHTSA

A series of 38 human cadavers tests has been conducted by researchers at the Medical College of Wisconsin and at the Vehicle Research and test center [31]. Both institutions used a Heidelberg-type side impact test apparatus as described in the previous section. The loading wall surface consisted of four plates instrumented with eleven uniaxial load cells. The loading surface was configured such that the upper plate contacted the mid-thorax, the middle plate contacted the abdomen, and the lower plate the pelvis. The upper edge of the thoracic plate was 40cm vertically from the middle of the seat such that the shoulder of the cadaver did not contact the plate. Thus, these experiments can not be used to investigate shoulder response, but they can be a useful tool to predict whole body response and, in that way, will provide the shoulder with accurate boundary conditions. The experimental data are not yet available at TNO.

3.4 Upper extremity experiments

The experiments found in literature can be roughly divided in two classes: impact-related experiments with pendulums and airbags, and mechanical segment experiments.

3.4.1 Arm impacts

Palaniappan *et al.* [32] presents three different experiments which they have performed to evaluate their finite element model of the human arm: (i) free swing tests, (ii) pendulum impact tests, and (iii) airbag tests.

The pendulum impacts can be used to evaluate kinematical behavior of the upper extremity and with the use of injury criteria found in literature (like maximum lower or upper arm accelerations) injury can be predicted. The posterior side of the arms of a cadaver was impacted by a 6.44 kg pendulum with a rectangular, flat surface. A load cell behind the flat plate measured the impact load and an accelerometer on the plate recorded the pendulum acceleration. From the tests, angle of rotation histories of the upper and lower arm relative to the inertial space were derived. The model of the set-up is shown in Figure 3.3.

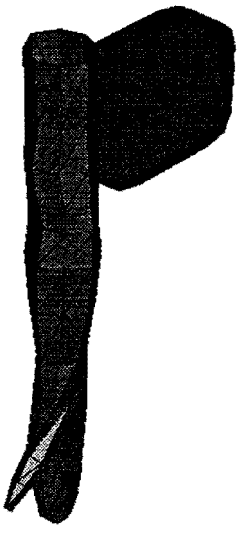

Figure 3.3: Model set-up of the arm pendulum impact.

Several researchers have presented their experimental results of airbag interactions with the upper or lower arm [32, 33, 34, 35, 36, 37, 38]. However, these experiments only show injury potential and can not be used to evaluate the arm model due to a lacking correct description of the airbag loading.

3.4.2 Segment tests

Much research has been performed using isolated components to examine mechanical behavior and injury tolerance of the humerus, lower arm, elbow and wrist. The advantage of component testing is that it offers a controlled experiment in which know loads are applied to a specific segment. A thorough literature research on these experiments can be found in Duma's thesis [8].

Chapter 4

Existing models

After a short description of mathematical modeling techniques generally applied in the automotive research, existing shoulder models (using these techniques) are presented in Section 4.2. Current upper extremity models are described in Section 4.3, followed by a discussion in Section 4.4.

4.1 Modeling techniques

Mathematical models of the biomechanical system have proven to be a strong tool in research of the functionality of the shoulder complex and impact related injuries. *Global* mathematical modeling, i.e by means of multibody techniques, of the real human body allows the study of aspects like body size, posture, muscular activity and post-fracture response. It enables evaluation of vehicle safety in early design stages, and is very effective for design optimization. Multibody models consist of rigid bodies interconnected by kinematical joints, and are defined by the geometrical properties, the types of joint, inertial properties and initial/boundary conditions. Due to a relative small number of degrees of freedom in the model, CPU time is small and costs are low.

More *detailed* mathematical modeling, i.e by means of finite element techniques, allows analysis on a material level, and is very effective for research purposes. Finite element modeling is applied to simulate structural behavior by reducing a continuum to a discrete numerical model. Because of the high number of degrees of freedom, the use of finite element techniques requires much more computational time and hence, results in higher costs. Furthermore, the definition of finite element models needs a high amount of parameters, which are often not available.

Thus, in case we are not interested in structural behavior, i.e. stresses and strains inside structures, but rather the global system behavior, multibody modeling is an appropriate technique. For in-depth research of structural behavior of systems finite element modeling is applied.

TNO Automotive has developed a mathematical simulation program to perform crash safety analyses of vehicles and occupants. The program, called MADYMO, combines both multibody and finite element techniques. The calculations presented in this report are performed with MADYMO version 5.4.1.

4.2 Shoulder models

Huang

Huang *et al.* [39] developed a three-dimensional rigid body model of human occupants in side impact, which was evaluated against a series of 17 cadaver side impact tests conducted at Wayne State University. Model parameters were chosen to yield human-like responses at the level of the shoulder, thorax, abdomen, and pelvis. The shoulder model is a very simplified description of the human shoulder. The humerus is directly connected to the thorax by a ball-and-socket joint, ignoring the functionality of clavicle and scapula. Deformations are not allowed in the shoulder girdle.

They showed with their model that the shoulder has a major protective function to the thorax. Without a shoulder and arm model, thorax injury criteria like TTI (thoracic trauma index) and VC (viscous criterion) could not be estimated correctly. In order to predict body deformations, they also developed a finite element model. The model was focused on thorax responses and the shoulder region was only modeled roughly. Several meshes for the shoulder were evaluated, but none of them was satisfactory [40].

Lizee

Lizee *et al.* [41] developed a finite element human model, including a simplified shoulder geometry, for predicting human responses and kinematics in the frontal, lateral and oblique impact direction (see Figure 4.1). As a result of a coarse shoulder mesh, the model is only applicable for kinematical evaluations. The shoulder model was evaluated with results of pendulum impacts performed by Meyer [42].

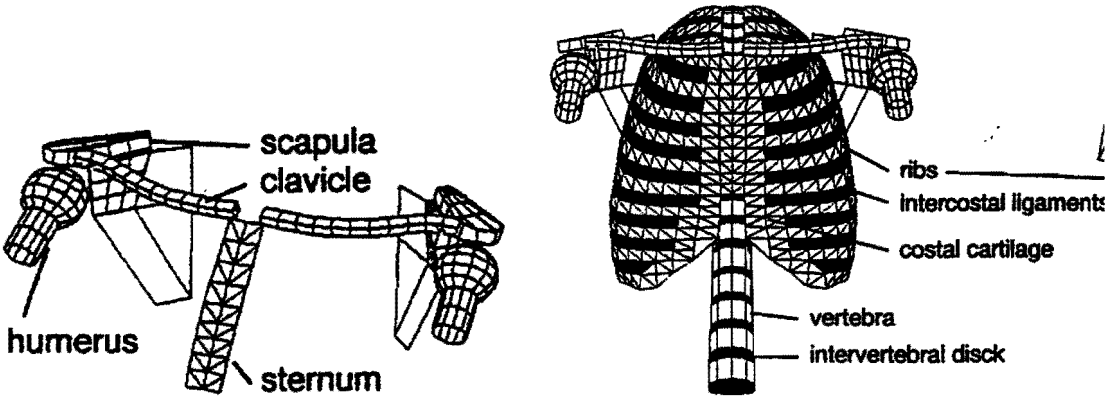

(a) Shoulder bones

(b) Frontal view of thorax and shoulder model

Figure 4.1: View of the finite element model of Lizee *et al.* [41].

Jost & Nurick

Jost and Nurick [43] developed a human body model for the purpose of simulating injury mechanisms due to vehicle side impacts. They combined the finite element model of Huang with the more advanced thorax model of Plank [44]. The model consists of skeletal bones (see Figure 4.2) and surrounding soft tissues. The bone material, muscles and surrounding tissues are assumed to be purely elastic. The internal organs are modeled by a visco-elastic material. The shoulder, i.e. clavicle and scapula, are modeled accurately. Muscles and ligaments surrounding the shoulder complex are modeled by volume-, shell- and membrane-elements. The biofidelity of the shoulder region is evaluated with pendulum impacts performed at Association Peugeot-Renault. There is a satisfactory correlation for the first 25ms. For contact times beyond 25ms the impact peak forces are larger than the test results.

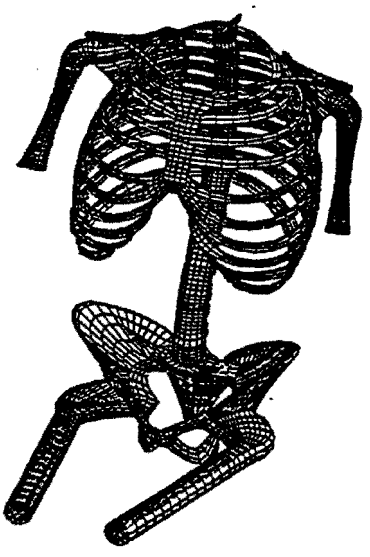

Figure 4.2: View of the finite element skeletal model of Jost and Nurick [43]

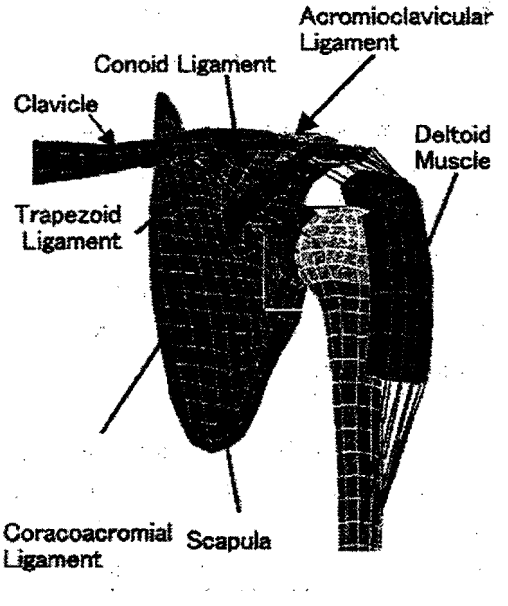

Figure 4.3: View of the finite element shoulder model of Iwamoto *et al.* [45]

Iwamoto

Iwamoto *et al.* [45] developed a finite element model of the human shoulder and integrated this model with a human thorax model. Detailed descriptions of the cortical and trabecular bone of the clavicle, scapula and humerus are included (see Figure 4.3). Major ligaments and muscles are also included to construct the articulations. Comparing model results against the cadaver tests conducted at Wayne State University showed that the shoulder is too compliant.

Haug

Haug *et al.* [46] reported a combined rigid body/finite element human body model including all separate bones and articulations. They used sliding contact interfaces between the scapula and the ribcage to model the interaction between scapulae and thorax. They also added passive muscles (non-linear beam elements) and evaluated the model against cadaver side impact sled tests performed at the University of Heidelberg. The model was evaluated against the gross motion of the shoulders and can not be used to analyze detailed interactions [45]. The validation results are not available.

Van Hassel

Van Hassel [47] proposed a rigid body model of the shoulder, including all separate bones and articulations (see Figure 4.4). The load transfer from scapula to thorax is modeled by force models at several rib levels. The model shows acceptable performance for lateral evaluations. However, several model parameters are not experimentally derived and the model is not evaluated for other directional impacts. Van Hassel also investigated the effect of passive muscles. He did not adapt the joint characteristics (in which muscle and ligament effects are lumped) after adding the muscles. Therefore, his conclusion that de shoulder model is not sensitive for muscular activity is not correct.

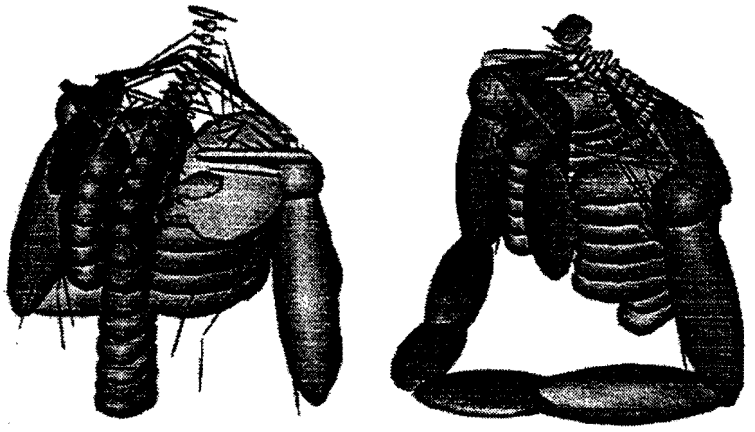

Figure 4.4: View of the multibody shoulder model of Van Hassel

4.3 Arm models

Palaniappan *et al.* [32] developed a finite element model of the human arm, including upper arm, lower arm and hand and corresponding joints in order to model airbag interactions. All bones are modeled as elastoplastic shell elements with equivalent thickness. The outer skin is modeled by elasto-plastic shell elements with constant thickness. The hand was modeled by rigid bodies. Free swing tests, pendulum impact tests and

airbag tests were used to validate the arm model. Since most properties were tuned to the freeswing and pendulum experimental results, the response of the model corresponded well with the experiments. The model showed promising results for the airbag experiments.

Pelletiere [48] developed a finite element model of the long bones of the human arm in order to study fracture mechanisms. Fracture mechanisms are modeled by element deletion. He was not able to predict crack propagation accurately and he suggests to use a more dense mesh.

4.4 Discussion

It is clear from literature that there is lack of validation data for the shoulder region. Interest has mainly been focused on other, more vulnerable body parts, thereby ignoring the interaction of these body parts with the shoulder region. Huang *et al.* [39] already stated that the shoulder could be protective to the thorax region during side impacts.

- The lack of experimental data is the reason that all shoulder models are only validated for the lateral impacts and none of them is validated for frontal, rearward or vertical loading conditions.
- A next result of this lack of validation data is that even the more detailed, finite element models are 'only' validated for the global kinematic response. At this level of validation, these finite element models do not provide more information than could have been provided by multibody techniques.
- Another topic of attention in these finite element models is the choice of the material parameters. Many of these parameters were obtained by adjusting until a good fit of the experimental data was achieved. Some values were even chosen in order to avoid numerical instabilities.
- The general objective of all models described in the previous sections was an injury prediction capability. However, none of the models has proven prediction capability for any injuries.
- None of the existing models pretended to have the objective to develop a multidirectional biofidelic response.

So, due to a lack of experimental data all shoulder models are validated for the kinematical behavior in the lateral direction. For most models this has been done with finite element techniques. Of course, this approach is very useful when we are interested in the detailed structural behavior of parts. But, since existing experimental data only allow validation of global entities like displacements, accelerations and forces, the - less time consuming - multibody approach is chosen in this study. Because of the existing model approach and reasonable response results, the shoulder model of Van Hassel is used as basis for the multibody model described in this report. Several model parameters in this model will follow from finite element simulation and experimental results on segment level.

Chapter 5

Multibody model

In this chapter the multibody (MB) models of the shoulder complex and upper extremity are described. In order to provide these models with accurate boundary conditions, these models are implemented in the mathematical human model developed at the TNO Crash Safety Research Centre. A description of this model can be found in [20] and [49].

5.1 Shoulder model

The multibody approach is chosen for the the shoulder model. Section 5.1.1 describes the model set-up. The choice of model parameters is presented in Section 5.1.2 and the modeling strategy with respect to deformations are described in Section 5.1.3.

5.1.1 Model set-up

A schematic view of the is MB shoulder model is shown in Figure 5.1. The clavicle, scapula and humerus are represented as rigid bodies connected by kinematic joints (numbers refer to numbers in Figure 5.1):

1: The sternoclavicular articulation between the medial end of the clavicle and the manubrium (upper part of the sternum)is modeled by a free joint - representing six degrees of freedom - with 3D rotational and translational force models. The characteristics of the 3D rotational force models are a representation of the resistive properties of the surrounding tissues (ligaments, muscles and other soft tissues) against relative rotations of the connected segments. The characteristics of the 3D translational force models are a representation of the compliance of the clavicle and therefore, they are a measure for clavicle deformation. Derivation of the translational characteristics is presented in section 5.1.3.

2: The acromioclavicular articulation between the acromion of the scapula and the distal end of the clavicle is modeled by a spherical joint - representing three degrees of freedom - with a 3D rotational force model.

3: The glenohumeral articulation between the humerus head and the scapula is modeled by a spherical joint with a 3D rotational force model (cardan restraint).

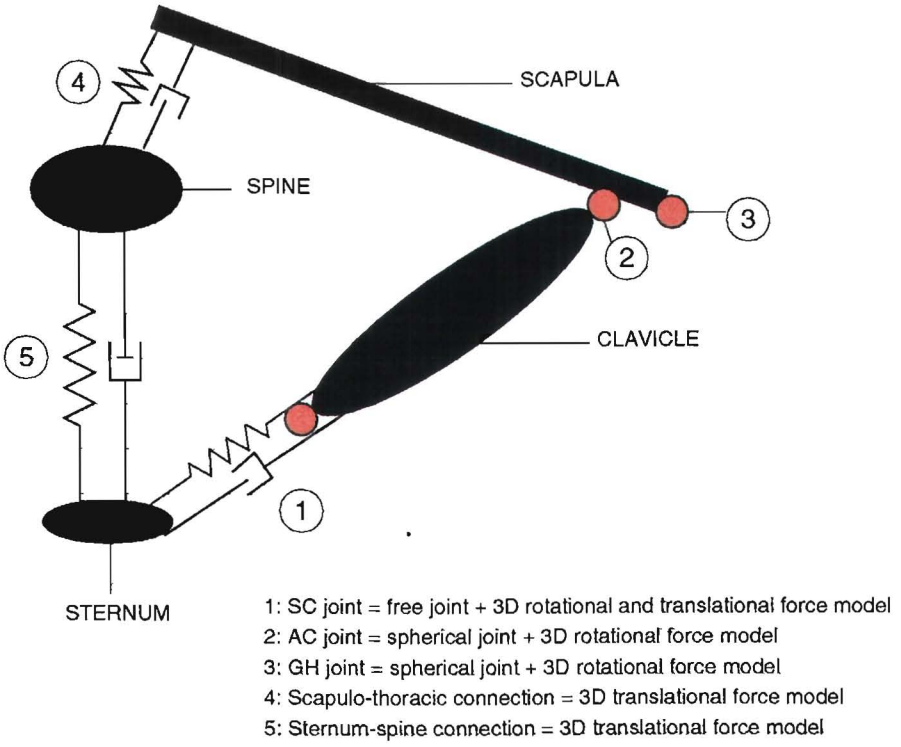

Figure 5.1: Schematic set-up (top view) of the multibody shoulder model.

4: In the real human body, the scapula contacts the thorax; the thoracoscapular connection. Active and passive muscle force is needed to maintain this contact and to stabilize the shoulder girdle. These complex interactions are modeled as a set of passive force models. The medial ends of the scapulae are supported on the spine with force models at two vertebral levels. The lateral stiffness of these force models are negligible in order to allow a 'sliding movement' of the scapula. The stiffness in anterio-posterior direction is relative stiff in order to model the real-life support of the scapula on the ribcage.

This means that the load transfer from shoulder to spine is modeled by the skeletal connection (humerus - scapula - clavicle - sternum - spine) and by these additional force models (humerus - scapula - spine). It would be more accurate to model this last connection by a sliding mechanism as described by Van Hassel [47]. He defines a thoracic gliding surface over which the scapulae are allowed to slide. The scapulae are 'pressed' against the thorax by passive force models. Since an accurate geometrical description of the thorax is not available at this stage, this method is not applied. As soon as a more accurate, deformable thorax geometry will be available, attention has to be paid to this subject. Figure 5.2 shows the distribution over the different load paths due to a dynamical lateral load on the shoulder model. The major part of the force will be transmitted through the skeletal connection.

5: In the human body the manubrium (upper part of sternum) is connected to the ribs, but for reasons, explained in Section 5.2, this is not possible in the model. Therefore, the

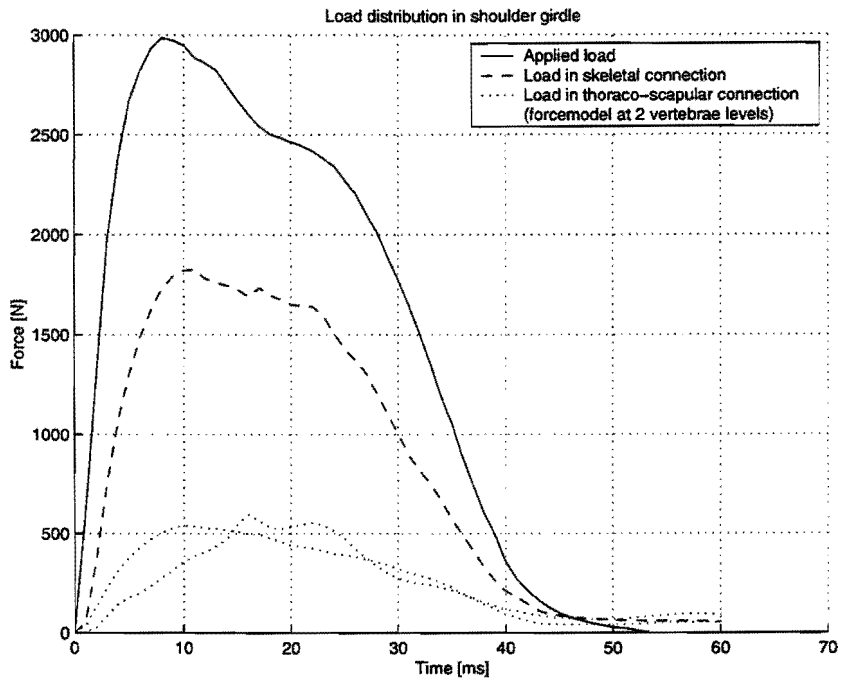

Figure 5.2: Distribution of a dynamical shoulder load over the different load paths to the spine.

upper sternum is connected to the spine by a free joint. Rotations of the sternum with respect to the spine are suppressed by relative stiff rotational force models. The compliance of the thorax between the sternum and the spine is modeled by 3D translational force models. The stiffness of this connection is derived with simulations on a finite element thorax model. This derivation and the results are presented in the section 5.1.3.

Geometry

The geometrical properties, i.e. joint locations, locations of center of gravity and skin geometry, have been derived from the RAMSIS anthropometric database [6]. The position of the glenohumeral and acromioclavicular joints had to be adjusted, because in RAMSIS the position of both joints coincides.

Mass properties

The masses and inertia properties of the segments are based on the RAMSIS anthropometric database and are presented in Table 5.1. Note that the products of inertia are zero, because body parts are assumed to be symmetric around the main inertial axes.

Body	Mass $[kg]$	Moment of inertia $[kg \cdot m^2]$			Product of inertia $[kg \cdot m^2]$		
		I_{xx}	I_{yy}	I_{zz}	I_{xy}	I_{xz}	I_{yz}
Clavicle	0.25	0.002	0.001	0.002	0.000	0.000	0.000
Scapula	0.10	0.001	0.001	0.001	0.000	0.000	0.000
Humerus	1.65	0.01	0.002	0.01	0.000	0.000	0.000

Table 5.1: Inertial properties of the clavicles, scapulae and humerus, based on the RAMSIS anthropometric database[6].

5.1.2 Joint characteristics

Rotational joint characteristics are implemented by means of three dimensional, rotational force models. The joint characteristics are based on literature data on human passive joint properties (see Chapter 2).

Free range of motion

The range of motion of the articulations is based on the RAMSIS anthropometric database [20] and Dempster's cadaver experiments [19] and is presented in Table 5.2.

Joint ranges of motion [°]				
	SC joint	AC joint	GH joint	Total
ϕ(x)	*40*	**30**	*130*	200
θ(y)	*20*	**30**	*140*	190
ψ(z)	*50*	**40**	*150*	240

Table 5.2: Ranges of motion of the sternoclavicular, acromioclavicular and glenohumeral joints of the shoulder complex ($\phi(x)$ upward/downward rotation about anterior-posterior axis; $\theta(y)$ axial rotation about medial-lateral axis; $\psi(z)$ forward/rearward rotation about superior-inferior axis) based on Dempster (**bold**) [19] and RAMSIS (*italic*) [20]

Rotational stiffness characteristics

Rotational resistive stiffnesses within the range of motion are assumed to be negligible; stiffnesses near the voluntary range of motion, are based on experiments with volunteers [23, 24]. They measured rotational stiffnesses in the order of 100 Nm/rad. The rotational stiffness for forced excursions of $0-3°$ beyond the voluntary range of motion is 100 Nm/rad. Research results of resistance parameters for more severe excursions are not found and have been chosen to be 1000 Nm/rad. Some data on rotational damping properties are provided by Engin [25].

These rotational characteristics are evaluated with the use of volunteer experiments of Engin [24]. The upper arm, initially spread to the side, was forced to rotate quasi-

statically: (i) about the sagittal axis (X-rotation) resulting in abduction of the arm; (ii) about the transverse axis (Y-rotation) resulting in axial rotation of the arm; and (iii) about the longitudinal axis (Z-rotation) resulting in flexion of the arm. In this way the combined stiffness and combined range of motion of the three shoulder joints and their force models is tested. In Figure 5.3 the relation between the passive resistive moment and the rotation angle of the arm is presented. From this figure, it is clear that the rotational stiffness functions are in the correct order of magnitude. The stiffness functions for axial rotations of the arm are a little too stiff and have to be decreased. For abduction and extension the model overestimates the free motion range. This will not occur for adduction and flexion due to contact definitions between the arm and the thorax region.

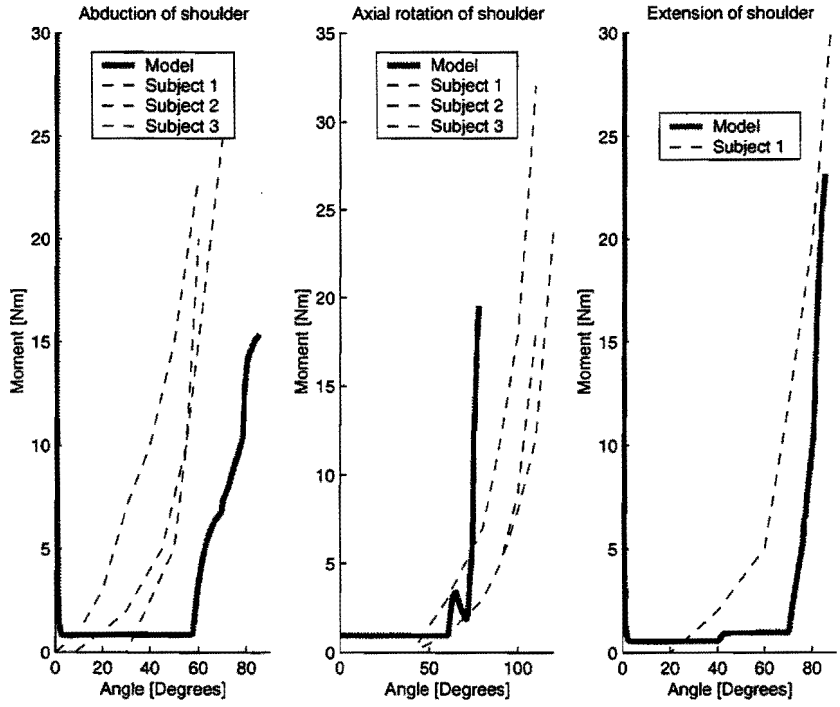

Figure 5.3: Moment - Angle relation of the shoulder complex for rotations about the principal axes; solid lines represent the model results, dashed lines represent experimental results of Engin and coworkers [24]

These results prove that it is possible to distribute the total motion range of the arm over the separate articulations. This enhances the biofidelity of the model, but one might question the applicability during positioning of the arm, since all initial positions of joints need to be set separately. Furthermore, in the human body a rotation of the arm is a combined and simultaneous rotation in the glenohumeral, acromioclavicular and sternoclavicular articulations. This is often referred to as 'shoulder rhythm': when the arm rotates a certain angle, the scapula rotates at the same time with a fixed ratio of the arm rotation. In the model rotation of the arm is a successive rotation of the separate joints: First the glenohumeral joint is rotated until the end of the free motion range is

reached, followed by a rotation of the acromioclavicular, and finally the sternoclavicular joint. These successive rotations are visualized in Appendix C

5.1.3 Deformations

In reality, the clavicles, thorax and the sternum deform when the shoulder is loaded. These bones are modeled as rigid bodies and therefore they cannot deform. In order to predict biofidelic shoulder kinematics, these deformations have to be incorporated into the model. The deformation of the clavicle is represented by a 3D translational force model between the clavicle and sternum. The stiffness functions of this connection are derived with the use of finite element simulations and clavicle experiments. This derivation and the results are presented in this section.

A similar type of force model is used to model the connection between the manubrium (the upper part of the sternum) and the third vertebra of the spine in order to simulate thorax deformations. During a side impact loading the thorax will deform because of two loading conditions: First, there is a direct load transfer from the impacting object on the thorax, or from the impacting object on the arm resulting in a load on the thorax due to arm/thorax contact. Next, a load transfer takes place through the shoulder and the sternum on the ribcage. Both deformations will contribute to total shoulder kinematics. In the human body the manubrium is connected to the ribs, but for practical reason (see Section 5.2) this is not possible in the model and, hence only the deformation between the sternum and the spine caused by the skeletal connection (humerus-scapula-clavicle-sternum) is modeled. The stiffness functions of this connection are derived with the use of finite element simulations. This derivation and the results are presented here:

I. Derivation of thorax force model

A validated finite element thorax model by Van der Made [50] is used for derivation of the properties of the translational force model between the sternum and spine (see no.5 in Figure 5.1). The deformations resulting from this force model represent the deformation of the thorax with respect to the (rigidly supported) spine. Within the FE thorax model, sternum nodes in the sternal area were forced to translate quasi-staticly in the X,Y or Z-direction. The forces needed to accomplish these deformations are plotted against the deformations in Figure 5.4. In this same figure the force - deformation characteristics of the force models in the multibody model are illustrated.

II. Derivation of clavicle force model

The characteristics of the translational force model that represents clavicle deformation (see no.1 in Figure 5.1) are based on PMHS axial compression experiments on clavicle segments. Details of these experiments can be found in Section 7.2.4. The results of these experiments and the characteristics of the multibody force model are shown in Figure 5.5.

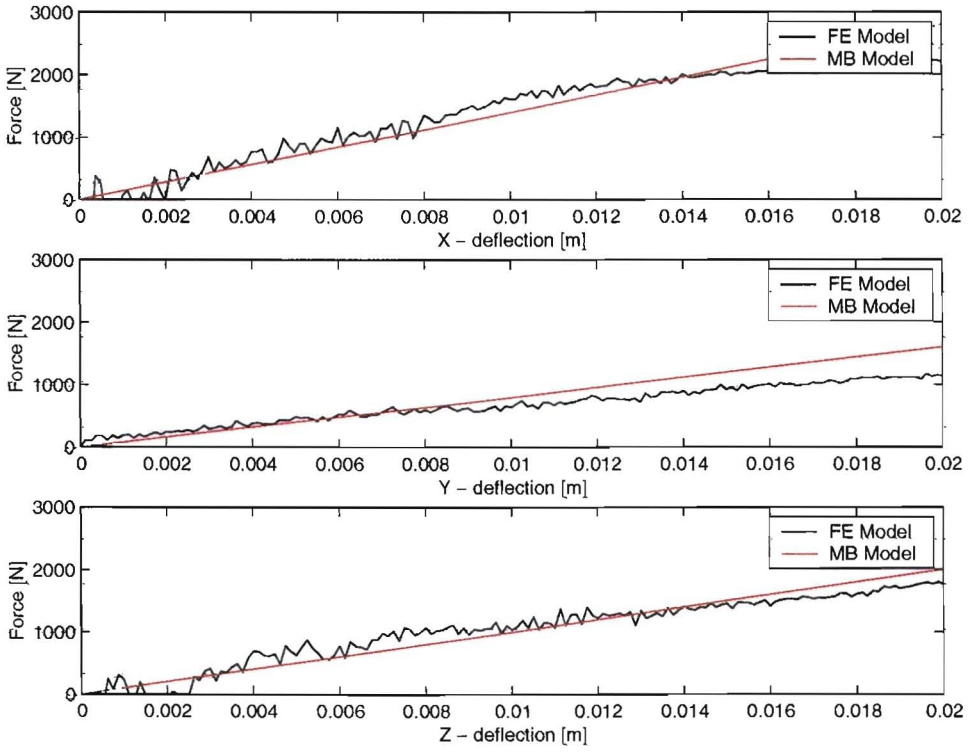

Figure 5.4: Force vs. deformation characteristics of Van der Made's FE thorax model and the characteristics implemented in the multibody model.

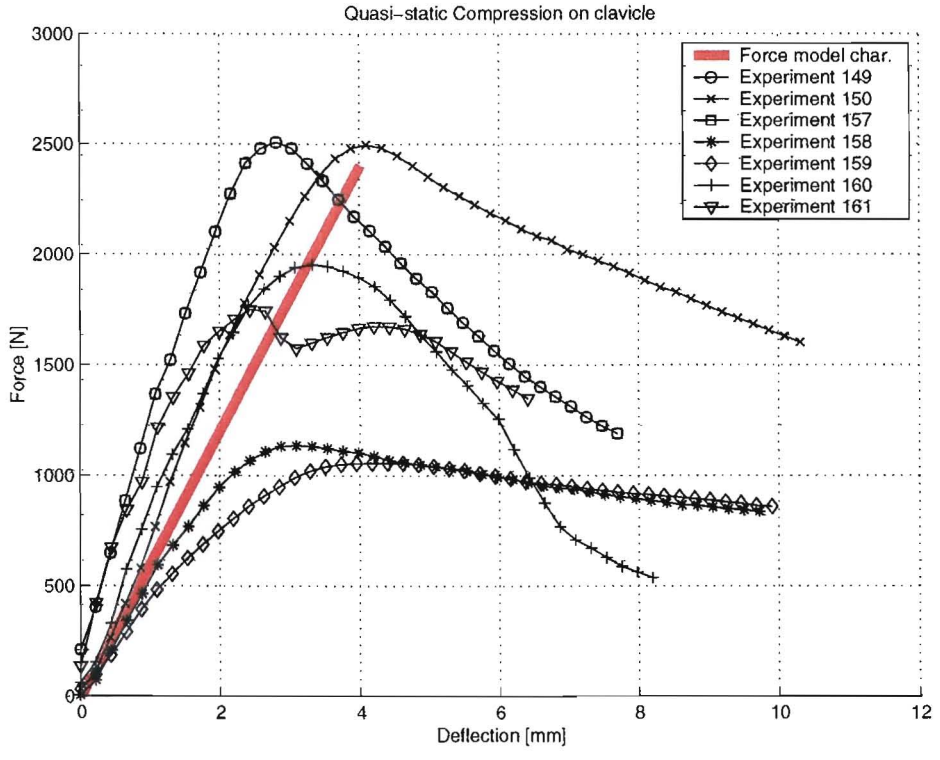

Figure 5.5: Force vs. deformation characteristics of the axial compression experiments on PMHS clavicles and the characteristics implemented in the multibody model.

5.1.4 Contact interactions

To describe accurately the load transfer from the skin and soft tissues to the load-bearing bodies, a skin geometry based on the RAMSIS database is applied in TNO's human model. This has been done by means of a facet surface description. This facet surface is defined by nodes, that are supported on the represented body segment. Though, the facet description in the shoulder region is relative rough and problems arise due to folding of the shoulder skin during arm rotations.

5.2 Thorax model

In this section the reason for not connecting the shoulder model to TNO's multibody thorax model is explained.

The thorax region in TNO's human body model consists of four flexible bodies. These flexible bodies describe 3D deformations with only a few degrees of freedom and therefore are CPU efficient [20]. The current flexible body approach has a few drawbacks when we want to support the shoulder model on the thorax model. The connection of the shoulder model on the thorax model could be established by a rigid connection between the upper sternum body and the frontal, mid-sagittal point of the most superior flexible body - the so-called 'support node' - , but:

- The flexible bodies do not allow lateral deformation of the support node. As a result a lateral shoulder load on the support node will not result in any lateral deformation of thorax region, but only in a rigid motion of the flexible bodies.
- Lateral deformation of the flexible bodies of the thorax will not contribute to shoulder kinematics, because the mid-sagittal part of the flexible bodies does not displace with respect to the spine.
- The most superior flexible body is connected to vertebra T7. This means that the flexible body thorax model ends at that level and the shoulder model will be connected at the lower sternum level instead of the upper sternum level.

Because of these major drawbacks it is decided to connect the clavicle directly to the spine until a better thorax model is available.

5.3 Arm model

The arm model presented in this section is an extended version of the arm in TNO's human model. The arm model is composed of rigid bodies for the upper arm, lower arm, midhand, fingers and thumb. For the lower arm, the radius and ulna are not modeled separately and therefore, the movement of these bones with respect to each other, i.e. pronation/supination, is lumped into the elbow joint. The masses and moments of inertia of these bodies are based on GEBOD [51], a program for the generation of human body properties, and are presented in Table 5.3.

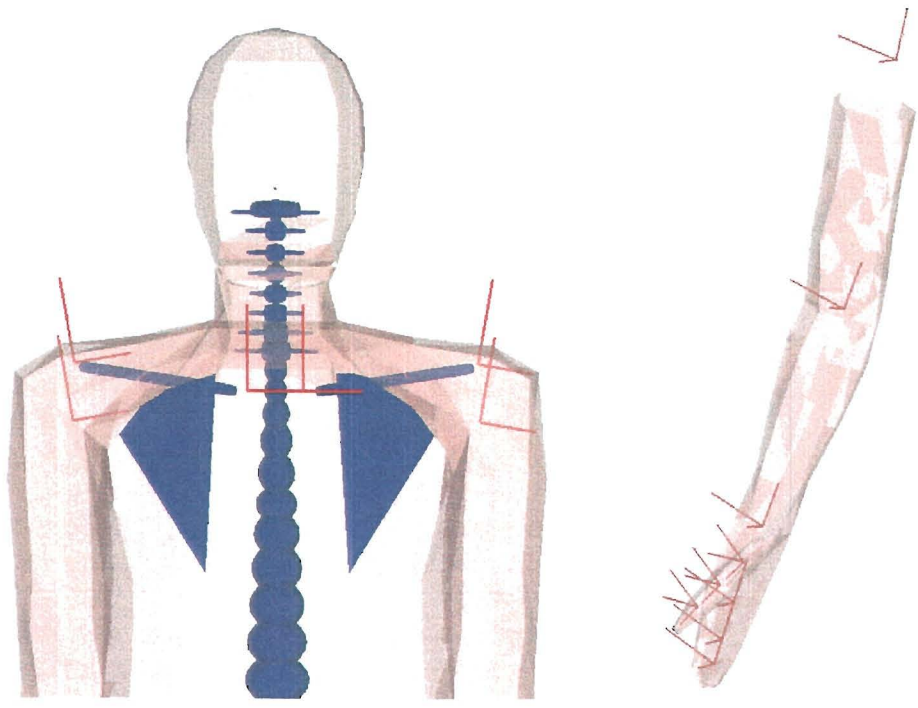

(a) Shoulder model (b) Arm model

Figure 5.6: The shoulder and arm model in frontal cross-sectional view. The coordinate systems indicate positions of the SC, AC and GH joints.

The elbow, wrist and finger joints are presented by spherical joints and thereby describe three rotational degrees of freedom. The model contains a three-segment representation of the combined fingers and a three-segment representation of the thumb. Degrees of freedom which are not allowed and excursions outside the free range of motion are limited by rotational force models. Besides flexion and extension, the elbow joint also allows supination and pronation (axial rotation) of the lower arm. It must be noticed that in real life these movements take place at the proximal and distal radio-ulnar joints. The wrist joint allows for flexion/extension and adduction/abduction. The wrist model combines the properties of the radio-carpal and metacarpal joints (see Chapter 2).

Body	Mass $[kg]$	Moment of inertia $[kg \cdot m^2]$			Product of inertia $[kg \cdot m^2]$		
		I_{xx}	I_{yy}	I_{zz}	I_{xy}	I_{xz}	I_{yz}
Lower arm	1.25	0.0077	0.0012	0.0077	0.000	0.000	0.000
Mid hand	0.23	0.001	0.001	0.001	0.000	0.000	0.000
Fingers	0.20	2.0E-5	2.0E-5	2.0E-5	0.000	0.000	0.000

Table 5.3: Inertia properties of the lower arm, hand and fingers, based on the GEBOD database[51].

Similar to the shoulder joints, rotational joint characteristics are implemented by means of three dimensional force models. The joint characteristics are based on literature data on human passive joint properties (see Chapter 2). The range of motion of the articulations is based on Kapandji [21] and Engin experiments [52] and is presented in Table 5.4.

Joint ranges of motion [°]			
	elbow	wrist	fingers
$\phi(\mathbf{x})$	150	170	135
$\theta(\mathbf{y})$	175	0	0
$\psi(\mathbf{z})$	0	60	30

Table 5.4: Ranges of motion of the elbow, wrist and (proximal) finger joints ($\phi(x)$ flexion/extension; $\theta(y)$ axial rotation; $\psi(z)$ adduction/abduction) based on Kapandji[21] and Engin[52]

Rotational resistive stiffnesses within the range of motion are assumed to be negligible; stiffnesses near the voluntary range of motion, are based on experiments with volunteers [23, 24]. They measured rotational stiffnesses within the range of 100 Nm/rad. The rotational stiffness for forced excursions of $0-3°$ beyond the voluntary range of motion is 100 Nm/rad. Research results of resistance parameters for more severe excursions are not found and have been chosen to be 1000 Nm/rad.

5.4 Spine model

The spine model in the TNO human model [49] has been validated for flexion/extension, lateral bending and axial compression/elongation. In order to evaluate the shoulder model under omnidirectional impacts, also torsional properties have to be implemented. The motion properties of the lumbar and thoracic spine are based on Kapandji [21]. Stiffness properties are based on Moroney [53] and De Jager [54]. The motion range of the lumbar spine (S1-T12) is $-9° \leq \phi \leq 9°$ equally distributed over the vertebrae. The motion range of the thoracic spine (T12-T1) is $-39° \leq \phi \leq 39°$ equally distributed over the vertebrae. Lumbar and thoracic torsional stiffnesses for intact spine segments are reported by Moroney. However, these results represent *in vitro*, quasi-static properties.

De Jager introduced a scale factor to represent the difference in stiffness between *in vitro* and *in vivo* joint behavior, as well as the increased dynamical stiffness. For axial rotation (torsion) this scale factor was found to be ca. two. This results in rotational stiffness of 1000 Nm/rad for the lumbar spine and 300 Nm/rad for the thoracic spine.

5.5 Discussion

- The shoulder model described in this chapter is based on the multibody shoulder model of Van Hassel. The following adjustments and improvements are performed:
  - Improved, biofidelic geometry;
  - Improved joint characteristics ;
  - Better understanding of deformation characteristics;
- A simplified description of the thoraco-scapular connection has been applied due to a lacking geometrical description of the thorax. In order to improve the movement of the shoulder girdle a better description of the movement of the scapula on the thorax wall is desirable.
- Muscles and ligament properties are lumped into the rotational and translational joint properties.
- The shoulder model consists of three joints with separate joint motion ranges. From a biofidelity point of view this is desirable. However, if the arm is being positioned in an extreme position, this positioning has to take place in all joints. From a applicability point of view this is not desirable.
- In the arm and shoulder model rotational damping has been implemented in the joint models. The damping properties are based on experiments and will be evaluated by free-swing and simple impact simulations. The question arises whether or not the influence of damping can be easily extrapolated to higher loading velocities.

Chapter 6

Model Evaluation

6.1 Evaluation multibody shoulder model

This section discusses the response of the global shoulder model with respect to the model requirements as described in Chapter 3. Section 6.1.1 discusses the pendulum simulations of Association Peugeot-Renault and Meyer. Section 6.1.2 shows the results of the simulations of the Wayne State University sled experiments.

6.1.1 Pendulum impact

Figure 6.1(a) shows the total force, i.e. elastic and damping force, acting on the shoulder resulting from the APR cylindrical impactor, as described in Section 3.2.

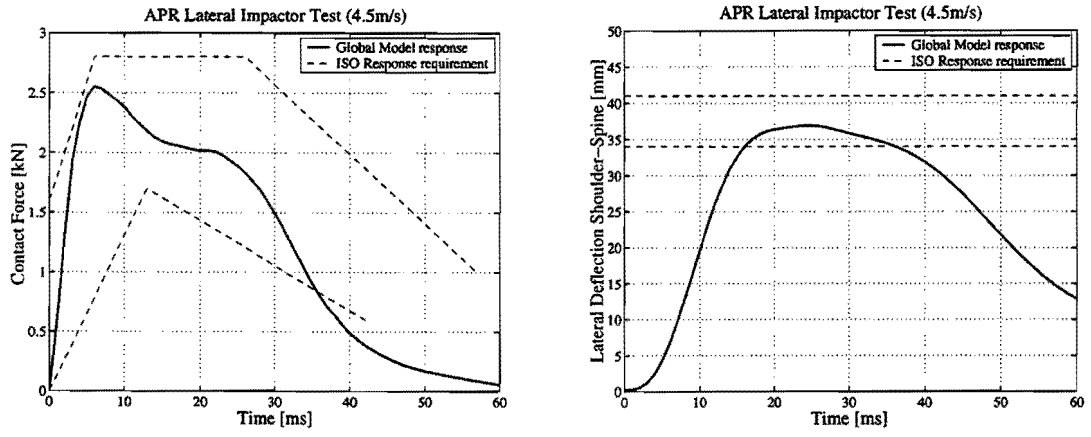

(a) Pendulum Force - Time

(b) Pendulum Deflection - Time

Figure 6.1: APR response of the global shoulder model relative to the ISO response requirements for the resulting contact force and the maximum relative displacement between shoulder and spine.

Figure 6.1(b) shows the relative lateral displacement between the impacted shoulder and the first thoracic vertebra T1. The maximum relative displacement, 37 mm, corresponds with the ISO requirement of 37.5 ± 3.5 mm.

Figure 6.2 shows the total force, i.e. elastic and damping force, acting on the shoulder as a result of the LBA square impactor. It is clear from this figure that the model underestimates the maximum contact force.

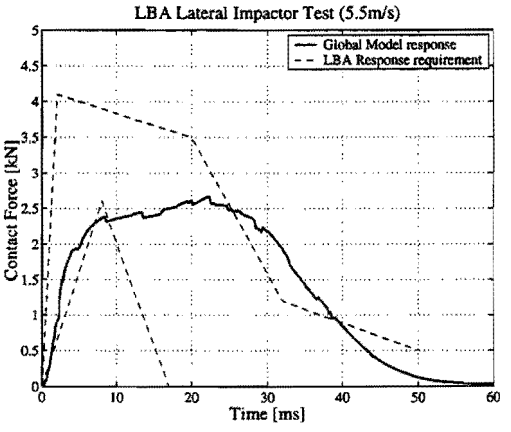

Figure 6.2: Response of the global shoulder model relative to the LBA response requirements for the resulting contact force.

When comparing the ISO and LBA response requirements, we can see a difference in the expected shoulder response. The LBA response requirement is stiffer than the ISO requirement. A clear cause for this can not be given, because the original reports and data of both experimental sets are not available. Despite of the different loading velocities - but the same mass - , both the APR and LBA model response show a similar maximum contact force.

6.1.2 WSU Sled impact

Figure 6.3(a) and 6.3(b) show the lateral displacement of the non-impacted acromion for both impact velocities. For both impact levels, the model experiences a comparable onset of displacement with the cadaver response. The maximum displacement is underestimated with 20% for the lower velocity and with 25% for the higher velocity. Acromion fracture in the cadavers can be an explanation for this.

Since the upper sternum is connected to the third thoracic vertebra, the kinematical behavior of this part of the spine has a major influence on the overall shoulder kinematics. Figure 6.4 and 6.5 show the results of the response of the first thoracic vertebra. Figure 6.4(a) and 6.4(b) show the acceleration response of the first thoracic vertebra. It is remarkable that for both impact velocities the experimental peak accelerations are equal. For the faster impact, the experimental and model response for the peak acceleration show a difference of 20%. For the lower impact, the experimental and model response show a difference of 50%.

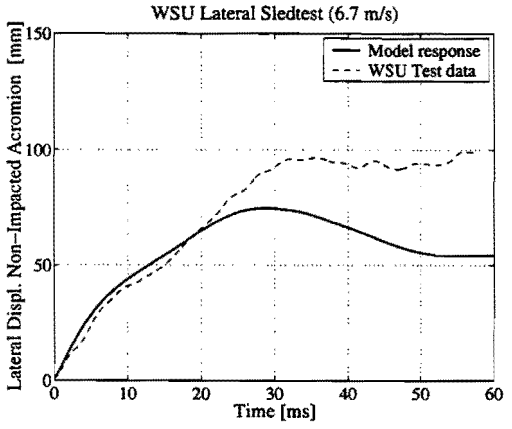

(a) Sled 6.7 m/s

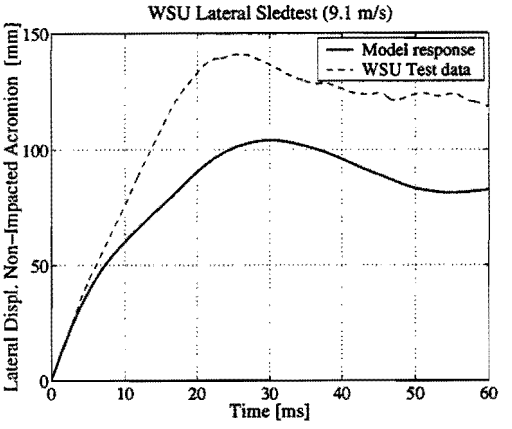

(b) Sled 9.1 m/s

Figure 6.3: Lateral displacement response of the non-impacted acromion relative to the experimental results of rigid wall sled impact tests performed at Wayne State University.

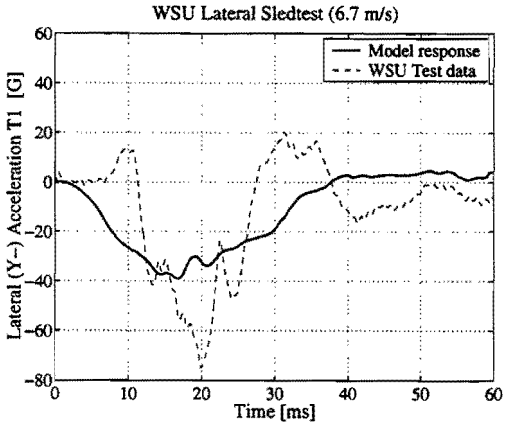

(a) Sled 6.7 m/s

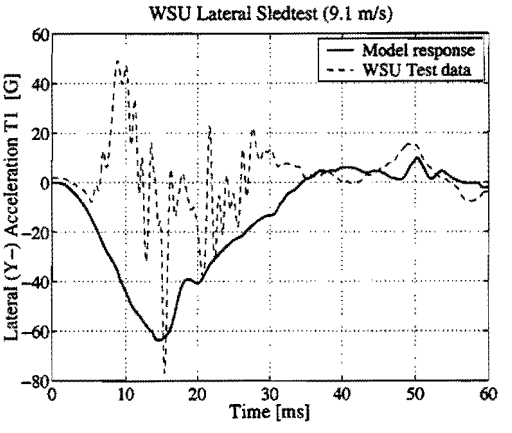

(b) Sled 9.1 m/s

Figure 6.4: Lateral acceleration response of the first thoracic vertebra T1 relative to the experimental results of rigid wall sled impact tests performed at Wayne State University.

Figure 6.5(a) and 6.5(b) show the displacement of the first thoracic vertebra T1. The lower rigid impact shows acceptable model behavior; the shape as well the peak of the displacement curve corresponds with experimental data. The peak displacement is overestimated with 30% for the higher impact and with 3% for the lower impact. Also a remarkable response at time 6 ms can be seen for both the displacement and accelerations. This can be ascribed to failure of the acromion (part of scapula), resulting in a lower displacement of T1.

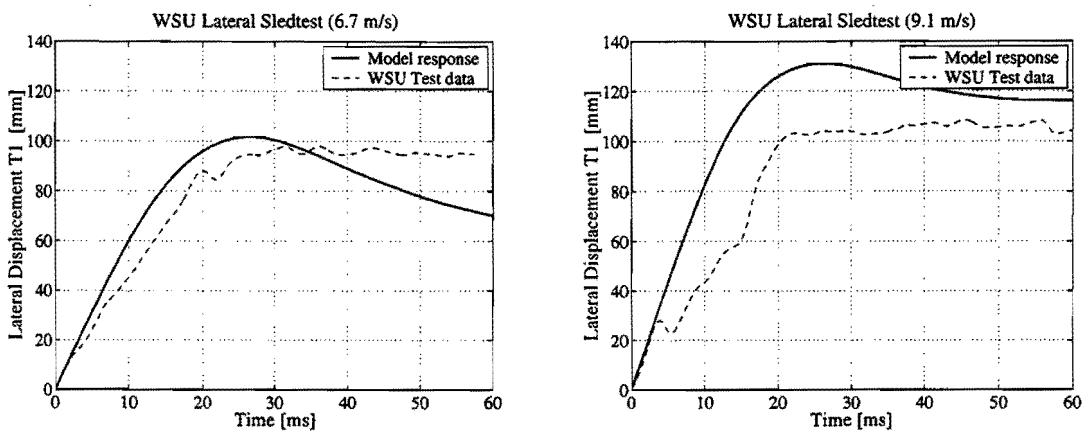

(a) Sled 6.7 m/s

(b) Sled 9.1 m/s

Figure 6.5: Lateral displacement response of the first thoracic vertebra T1 relative to the experimental results of rigid wall sled impact tests performed at Wayne State University.

Figure 6.6(a) and 6.6(b) show the total forces of the shoulder and thorax impact surfaces. The overall shape for both impact velocities are acceptable, but the maximum contact force in the lower impact is overestimated with 30%. The maximum contact force for the higher impact shows a difference of only 5%. The shoulder and thoracic region were combined for the experiments because of the large variation in the heights of the cadavers.

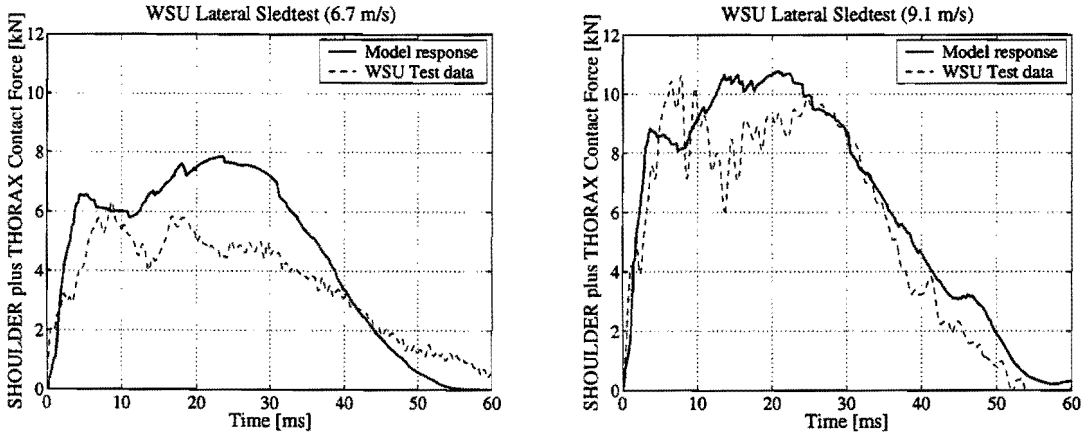

(a) Sled 6.7 m/s

(b) Sled 9.1 m/s

Figure 6.6: Shoulder plus thorax force response relative to the experimental results of rigid wall sled impact tests performed at Wayne State University.

6.2 Evaluation multibody arm model

Pendulum impact

Figure 6.2 shows the resulting movement of the arm as a result of a 6.44 kg impact on the posterior side of the upper arm. The angles are defined with respect to the inertial space and zero angles correspond to the arm hanging down. Note that the experimental data are based on *one* test on *one* subject. The model is capable of predicting the maximum shoulder and elbow angle within 5%. Furthermore, the model is capable of predicting the initial positive elbow angles. This can be seen as a measure for the inertial properties of the lower arm.

The correlation between the experimental and model response has been achieved by adjusting the damping properties in the joints until a good match with the experimental data is found. This resulted in a damping coefficient (in all directions) of 0.3 Nms/rad for the shoulder joint and 0.5 Nms/rad for the elbow joint. These values correspond with experimental results from Engin (see section 2.3.3), which are in the range 0.3 - 0.6 Nms/rad.

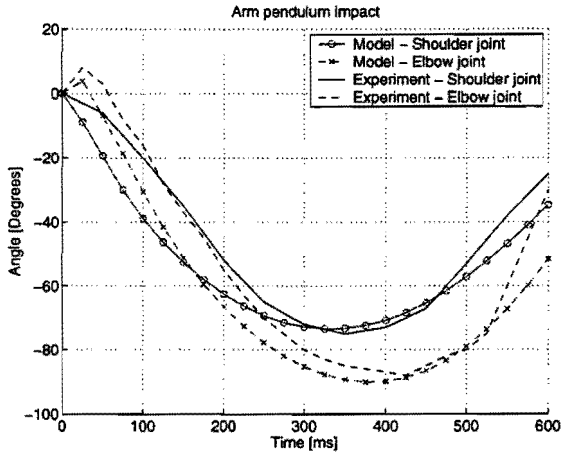

Figure 6.7: Response of the arm model relative to a 6.44 kg impact response for the resulting joint angles.

Freeswing tests

Figure 6.8 and 6.9 show the kinematics of the arm model subjected to forward/backward and lateral freeswings, expressed in inertial space angles again.

Good correlation between the model and the cadaver responses is achieved for the maximum angle during every cycle. But, the cycle times were different (Model: T=1.25s, Cadaver: T=1.1s). A reason for this is difficult to give since anthropometric data of the cadaver are not available.

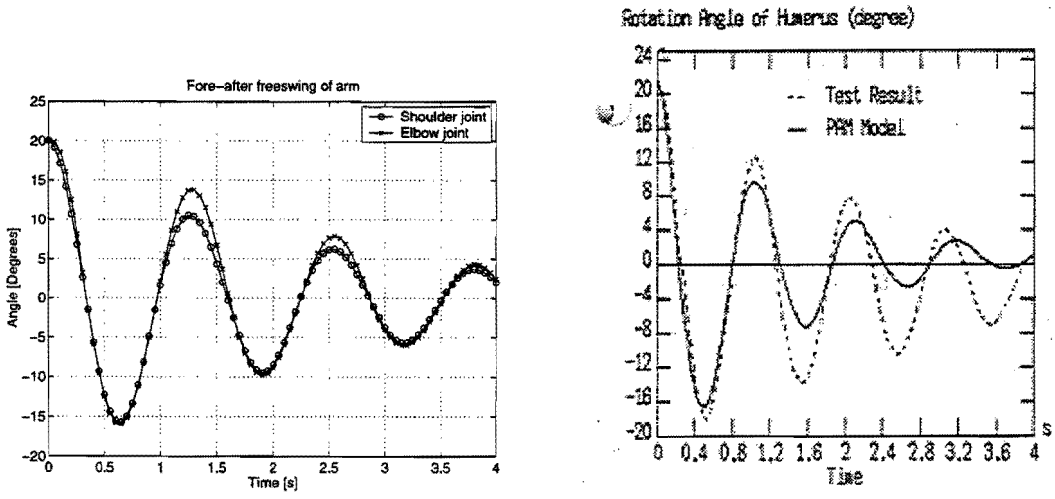

(a) Model response

(b) Experimental response

Figure 6.8: Shoulder and elbow angle response relative to the experimental results of **forward/backward** freeswing tests performed at Wayne State University (–).

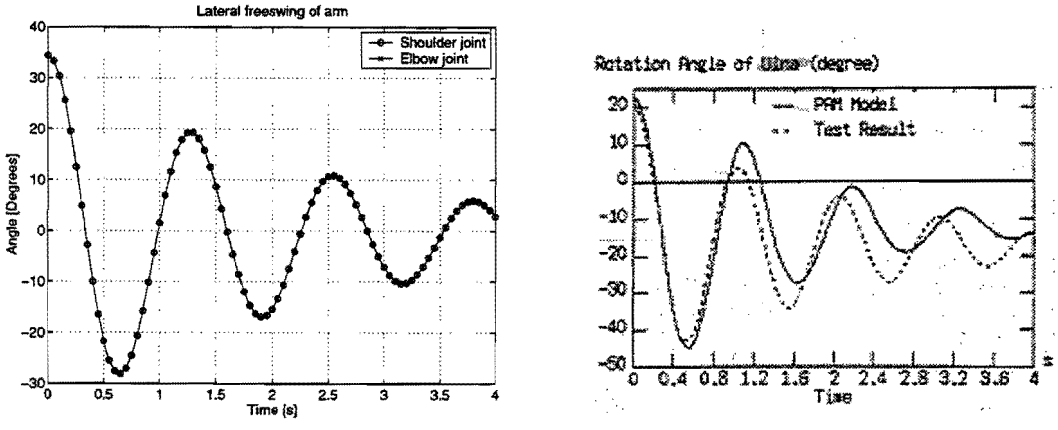

(a) Model response

(b) Experimental response

Figure 6.9: Shoulder and elbow angle response relative to the experimental results of **lateral** freeswing tests performed at Wayne State University (–).

6.3 Discussion

Lateral evaluation of the shoulder model has been performed using the APR and LBA PMHS pendulum tests and WSU PMHS sled tests. Considering the low number of subjects per experiment and the resulting experimental response uncertainties, it can be concluded that there is acceptable correlation between the model response and the experimental data. The model is capable to predict force versus time responses and global displacements and deformations of body structures, but:

- The APR and LBA sources give a different kind of force response requirement for lateral impact. Since the original test reports of the APR pendulum tests and the LBA pendulum tests are not available, it is not possible to define the better requirement.
- No clear explanation is found for the difference in the APR and LBA model responses. Although the tests are performed with a same mass (but different impactor geometry) at different impact velocities, both simulations show a similar maximum contact force and a different shape of the model response.
- The displacement of the impacted acromion in the WSU PMHS sled tests is underestimated by the model. This indicates that the force model that describes clavicle deformation is too stiff. Together with the good prediction of the relative displacement between shoulder and spine, this also indicates that the force model describing thorax deformation is too compliant.
- It is difficult to give conclusions about the acceleration response of vertebra T1 because of the remarkable experimental response. Although the model underestimates the experimental acceleration response with 50%, the displacement of vertebra T1 is predicted well.
- The WSU PMHS sled tests validation is based on two experiments at different impact speed. When analyzing these data, the reproducibility aspect should be considered. Generally, more reliable response requirements are needed and the amount of test data should be increased.
- Note that the experiments are performed with cadavers and do not represent behavior of a living human.

With the use of validated, global entities like displacements, accelerations and forces it is possible to define global injury criteria. To get a better understanding of the causes and mechanisms of injury, more detailed information is needed. In the next chapter a finite element clavicle model is integrated in a finite element thorax model in order to investigate local deformations and stresses.

Chapter 7

Finite element shoulder modeling

7.1 General

In order to get better understanding of the deformations occurring in the shoulder girdle during impact, more detailed analyses have been performed on segment level. First, the development of a clavicle finite element (FE) model is described. Next, this model is integrated in an existing FE thorax model by Van der Made, followed by a discussion of the results.

7.2 Clavicle model

The development of a FE clavicle is presented. This model will lead to an improved insight and understanding of deformation patterns and mechanisms.

7.2.1 Model description

The finite element clavicle model is based on a shell element description for the cortical bone (336 elements) and a solid element description for the trabecular bone (312 elements). The contact between both tissues is established by node sharing. This mesh is provided by the HUMOS project [55] and represents the clavicle of a 50^{th} percentile male person.

According to Granik and Stein [56] the stiffness and strength of the trabecular bone is much weaker than that of cortical bone. Although one might expect that trabecular bone can be neglected in a FE clavicle model, simulations showed (see Section 7.2.4) that the absence of trabecular bone within the clavicle model has a notable effect on the numerical response. To show the effect of trabecular bone, all simulations have been performed with two clavicle models: one with trabecular bone included, and the other without trabecular bone. In the latter case, the mass of this bone is incorporated in the mass of the cortical bone to account for inertial effects.

Since the thickness of the cortical bone is very irregular along and around the clavicle, it is hard to define the thickness of the shell elements. A biofidelic thickness of

the cortical bone is not available and therefore the uniform thickness of elements is adjusted to provide a good match to the results of the quasi-static three point bending experiments. This approach has the major disadvantage that, despite of the fact that global deformations can be predicted well, conclusions about local strains and stresses are difficult.

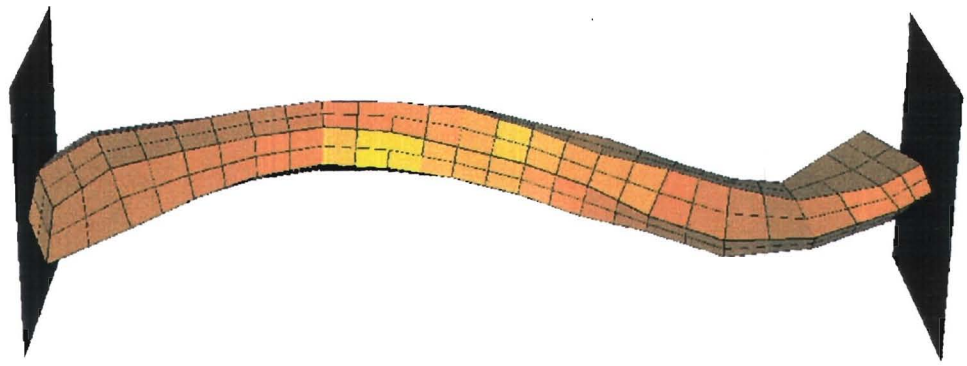

Figure 7.1: Finite element mesh of clavicle

7.2.2 Material properties

Within the scope of the HUMOS project a bibliographic study is performed about the material properties of biomaterials. A general conclusion was that bone properties are dependent on many factors and therefore data on mechanical properties of bone vary widely in literature. It is commonly accepted that bone is an anisotropic, non-homogeneous, rate-dependent and age-dependent material. Furthermore, it is generally established that bone properties vary according to type of bone (femur, tibia, rib, radius,..) and also according to the position within the bone (cortical bone and trabecular bone). Since in literature no data were found on the material properties of clavicle bone, experiments have been performed to acquire these data. Compression and three point bending experiments - static and dynamic - have been performed at the University of Heidelberg and similar results on rib tests have been analyzed by Van der Made [50].

These experiments on clavicles are simulated with three different clavicle models: (1) a model with a linear, isotropic, ideal elasto-plastic shell description for the cortical bone, (2) a model with a linear, isotropic, elastic shell description for the cortical bone and a linear, isotropic, ideal *elastic* solid description of the trabecular bone, and (3) a model with a linear, isotropic, elastic shell description for the cortical bone and a linear, isotropic, ideal *elasto-plastic* solid description of the trabecular bone

Based on available material properties, the cortical bone is described by an isotropic linear elasto-plastic material model. The HUMOS bibliographic study gives a Young's

modulus between 14 and 19 GPa for the cortical bone of long bones. Van der Made suggests a modulus of 16 GPa for cortical rib bone and Mow and Hayes [57] suggest 17.0 GPa. For the yield stress - the stress at which plastic deformation starts to occur - HUMOS suggests a value between 100 and 140 MPa.

It is difficult to give general material properties for trabecular bone because of its dramatic variation. Furthermore, the mechanical behavior is profoundly influenced by the apparent bone density. The density of trabecular bone is expressed in apparent density, i.e. the mass of bone tissue divided by the bulk volume of the tests specimen. According to Van Rietbergen [58] apparent densities range between 300 and 700 kg/m^3, Young's moduli range from 200 to 1300 MPa, and Poisson ratio's are in a range from 0.25 to 0.47. Since reported values of the yield stress vary even more, a value has been chosen related to the ratio of the Young's moduli.

Material models and model parameters used in the simulations for both type of bone are presented in Table 7.1.

Property	**Cortical bone**	**Trabecular bone I**	**Trabecular bone II**
	Ideal elasto-plastic	Ideal elastic	Ideal elasto-plastic
E-modulus [GPa]	16	0.5	0.5
Yield stress [MPa]	120	0	4
Poisson ratio [-]	0.3	0.4	0.4
Density [kg/m^3]	1850	600	600

Table 7.1: Applied material models and model parameters of the clavicle finite element model

7.2.3 Three-point bending experiments

Quasi-static tests

Quasi-static (loading speed 2.5 mm/min) experiments are conducted on a universal testing machine. The distance between the supports is 100mm and the radius of the supports and the impactor is 10mm. The results of the three-point bending experiments and the results of simulations with the clavicle model with and without trabecular bone are shown in Figure 7.3. The experiment numbers refer to the original test numbers presented by Kallieris [33] and anthropometric data can be found in Appendix D.

The stiffness of the elastic part (mean±std = 460±76 N/mm) and the maximum deflection (mean±std = 4.2±1.0 mm) are very varying. Kallieris showed that - for these experiments - there is no significant correlation between these parameters and the age of the cadavers. As mentioned before a biofidelic description of the thickness of the cortical bones is not available and therefore the uniform thickness of elements is adjusted to provide a good match to the results of the quasi-static three point bending experiments. The results showed in Figure 7.3 are obtained with a shell thickness of 1.5mm. The simulations show that both clavicle models are capable of predicting the elastic and

yielding behavior well. They also show that the trabecular bone has negligible effect on the elastic behavior, but as soon as yielding occurs becomes prominent.

Dynamic tests

Dynamic (loading speed 4m/s and 6m/s) experiments are conducted on a loading device with a spring accelerated impactor (2.35kg). The support distance and geometry of the supports and impactor is identical. The results of the dynamical experiments and the results of the simulations with the clavicle model are presented in Figure 7.5 and 7.6. Force output of both experiments and simulations is filtered with a CFC600 filter. Note that the constitutive behavior implemented in the clavicle FE model does not include strain-rate dependent effects.

In Table 7.2 calculated stiffnesses of the elastic part and the maximum deflections are presented together with the quasi-static values. Because of the high scatter of the results, it is not possible to make clear conclusions with respect to strain-rate dependency. In contrast with the general assumption in the literature, these experiments do not prove the hypothesis that clavicle bone has a strain-rate dependent stiffness and strength. Comparing the results from the quasi-static and dynamic experiments, a similar stiffness can be seen.

	Mean value	**Standard deviation**
	0 m/s	
Slope [N/mm]	460	76
Defl_{max} [mm]	4.2	1.0
	4 m/s	
Slope [N/mm]	414	117
Defl_{max}	6.0	2.0
	6 m/s	
Slope [N/mm]	375	73
Defl_{max}	4.3	1.7

Table 7.2: Calculated stiffnesses of the elastic part and the maximum deflections of the static and dynamic three-point bending experiments.

7.2.4 Axial compression experiments

Quasi-static axial compression experiments on whole clavicle specimens are conducted on a the same universal testing machine as is used for the three-point bending experiments. The ends of the specimens were embedded in a resin in order to prevent local deformations at the ends. Because of the curves in the shape of the clavicle, axial compression results in both compression and bending of the clavicle. The results of the axial compression experiments and the results of simulations are shown in Figure 7.4.

From this figure it is clear that the trabecular bone has a major effect on the response during axial loading. This effect is a result of the resistance of the trabecular solid ele-

ments against buckling of the cortical shell elements. The initial curves in the clavicle shape have a negative effect on the resistance against buckling. In the model without trabecular bone, there is no internal resistance against buckling of the cortical bone. Figure 7.2 shows the response with and without trabecular bone as a result of a prescribed compression. This problem can be solved by refining of the mesh in the curved areas. This mesh refinement results in lower initial angles between the shell elements. Since mesh refinement has a linear, negative effect on the critical timestep of the finite element algorithm, reinforcement of the shell mesh is applied by adding the trabecular bone.

(a) without trabecular bone

(b) with trabecular bone

Figure 7.2: Clavicle shape after a 7mm axial compression.

7.2.5 Discussion

The following things should be considered:

- Since a biofidelic thickness of the cortical bone is not available, an equivalent thickness of the elements is adjusted to provide the best match to the results of the quasi-static three point bending experiments. This approach has the major disadvantage that, despite of the fact that global deformations can be predicted well, conclusions about local strains and stresses are difficult.
- Although trabecular bone is neglected in many cases due to its weak mechanical properties, simulations showed that the absence of trabecular bone within the clavicle model has a non-negligible effect on the numerical response. Note that mesh refinement would decrease the reinforcing effect of the trabecular bone.
- The major mechanical effect of the trabecular bone is a strengthening effect of the cortical bone against buckling. In order to save calculation time it is worth considering to apply the trabecular bone only in the 'buckle-sensitive' areas.

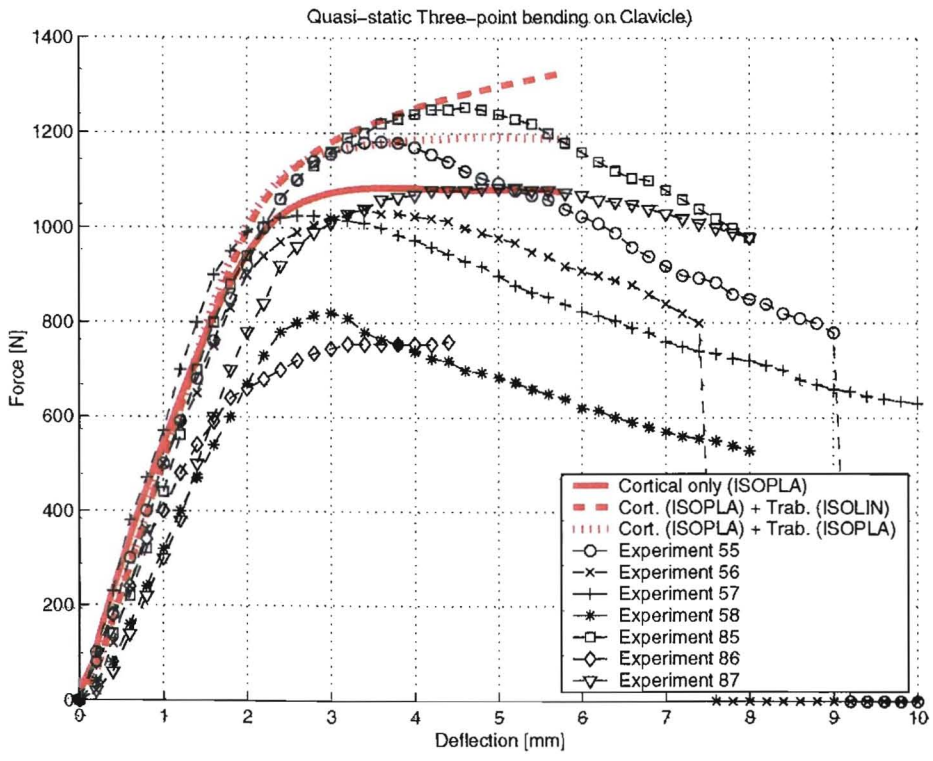

Figure 7.3: Force - Deflection curves of quasi-static three-point bending experiments and simulations on clavicle.

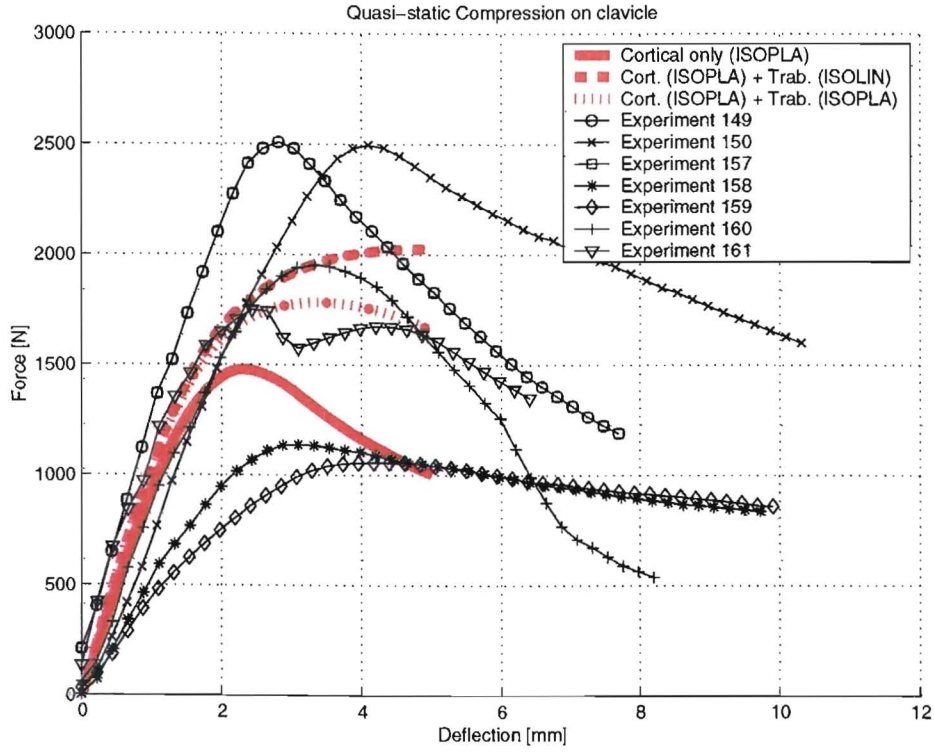

Figure 7.4: Force - Deflection curves of quasi-static axial compression experiments and simulations on clavicle.

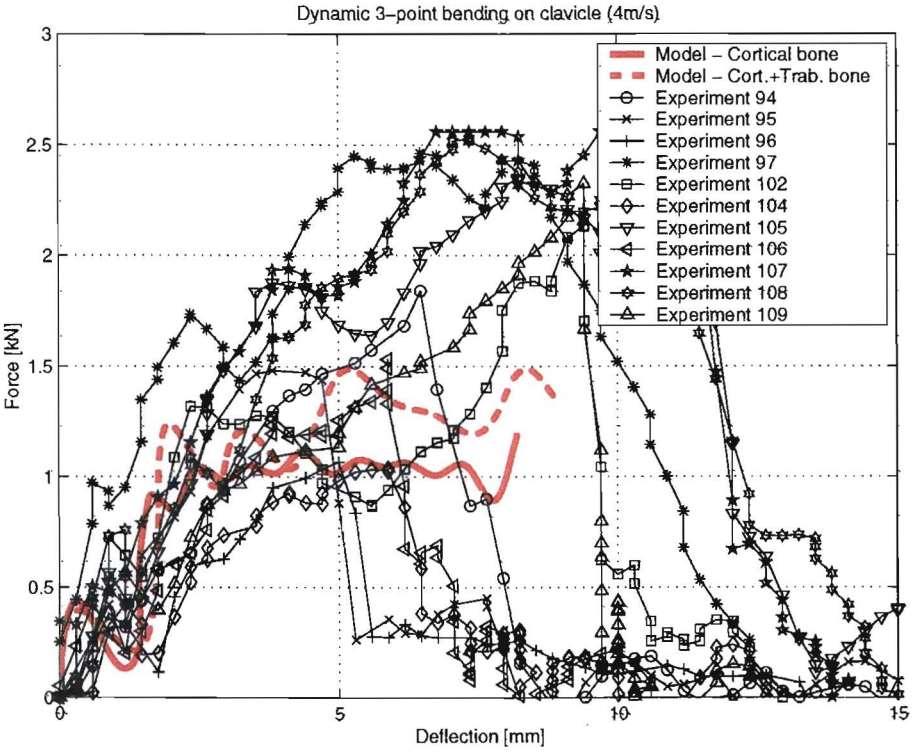

Figure 7.5: Force - Deflection curves of dynamic (4m/s) three-point bending experiments and simulations on clavicle.

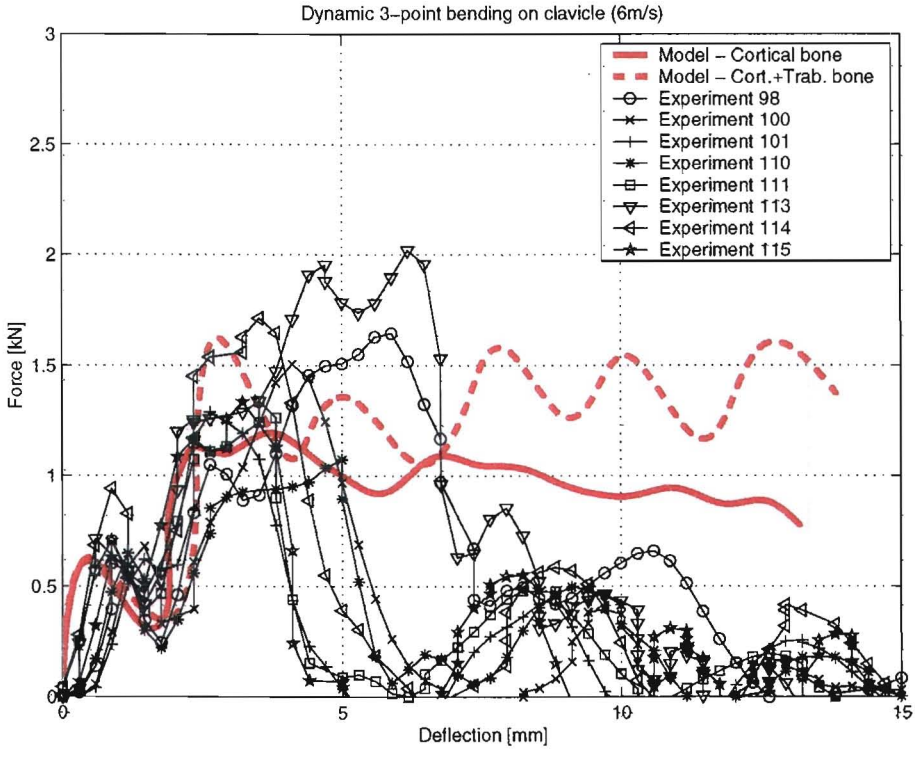

Figure 7.6: Force - Deflection curves of dynamic (6m/s) three-point bending experiments and simulations on clavicle.

- In contrast with general assumptions, the mechanical experiments performed by Kallieris show no apparent strain-rate dependency and age dependency for clavicle bone.

7.3 Integrated shoulder-thorax model

During lateral impact different structures in the human body will deform. In the previous section a FE clavicle model is presented. Now, this model is implemented in an existing FE thorax model by Van der Made and the deformations occurring during a lateral pendulum impact are investigated for both the finite element and multibody model. This will result in conclusions about: (1) the biofidelity of the translational force model between the sternum and the clavicle, which mainly represents deformations occurring in the clavicle; and (2) the biofidelity of the force model between the sternum and the spine, which represents the thorax compliance.

A description of Van der Made's thorax model can be found in his thesis [50]. His lateral validation showed that the thorax model was too compliant. According to Van der Made this was caused by the lack of a lower abdomen model in the model. Since at the sternal area the viscera are modeled and since during shoulder impact the thorax will be mainly loaded at this sternal and not at the abdomen level, it is expected that the response at the sternal level is predicted well.

The package MADYMO 5.4.1 has combined both multibody and finite element techniques. This also means that kinematical joints and force models can be used for joining two finite element models. The sternoclavicular connection between the sternum (FE thorax model) and the sternal side of the FE clavicle model is modeled by spherical joints with the same rotational force models as used in the multibody model. The acromioclavicular connection between the scapular end of the FE clavicle model and the multibody scapula is also modeled by spherical joints and matching force models. No changes have been made to the scapula and arm models. Kinematical joints are defined between two rigid bodies. Therefore, at both sides of the sternal area of the FE thorax model and at both ends of the FE clavicle model rigid bodies are defined. These bodies are rigidly connected to the matching nodes of the FE models.

Figure 7.8(a) shows the FE thorax and FE clavicle model integrated in the multibody human body model. When comparing Figure 5.6(a) and Figure 7.8(a), the difference in the distance between the arm and thorax is obvious. Initially, there is no contact between the arm and the thorax and all force is transmitted through the clavicle and scapula. As soon as there is arm-thorax contact, the force will be partly transmitted to the thorax directly. Comparing the multibody model and the FE model, this means that for the latter model relative more force is transmitted through the clavicle, resulting in higher deformations. In order to minimize this effect, a special contact algorithm is used, which specifies a virtual thickness of one of the contacting surfaces. In this way contact forces are generated before there is a visual contact between the surfaces.

7.4 Comparison FE and MB model

Both the multibody and the 'hybrid' model (FE thorax and FE clavicle model integrated in TNO's multibody human model) are subjected to the ISO lateral pendulum impact (see Section 3.2). A graphical overview of the response of both models is presented in Figure 7.8 - 7.9. The response of both models is compared in Figures 7.7(a)- 7.7(e). Note that the displacements and deformations are expressed with respect to the inertial coordinate system and due to rotations in the systems are not always a direct measure for axial segment deformation. The following can be concluded:

- As expected, the FE clavicle model *without* trabecular bone shows too compliant behavior, resulting in an overall, bad response.
- The response for the FE clavicle models *with* trabecular bone is identical, which means that - in this loading case - the maximum stress occurring in the solid elements (representing trabecular bone)of the FE clavicle model is below the yield stress.
- The MB model and the hybrid models *with* trabecular bone show comparable clavicle deformations.
- The MB model prediction of the lateral and frontal thorax deformation is compliant compared to the FE model. The MB force model characteristics are based on quasi-static simulations on the FE thorax model and do not take into account inertial and visco-elastic effects.
- The scapula is in all models modeled in the same way. In Figures 7.8 and 7.9 it can be seen that the kinematics of the scapula are different for both models. This means that the deformation pattern of the FE clavicle model has effect on scapula behavior.

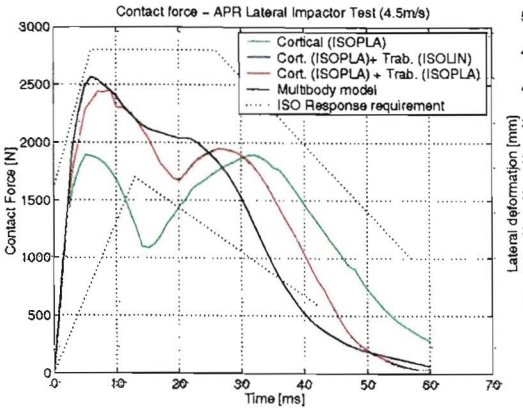

(a) Force vs. Time response

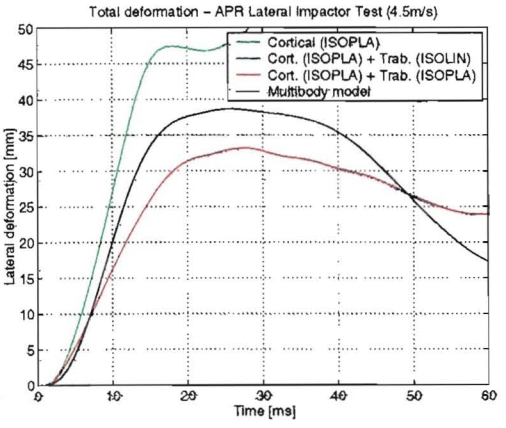

(b) Relative displacement shoulder-spine

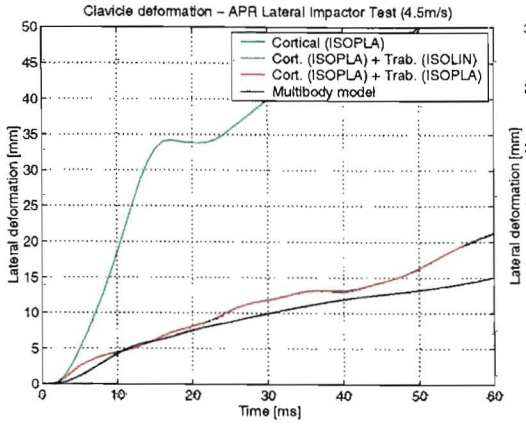

(c) Lateral deformation of left clavicle

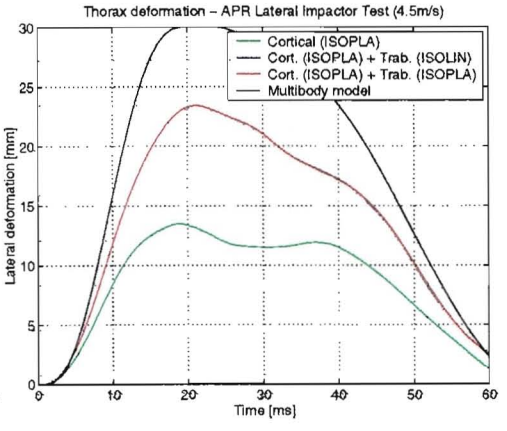

(d) Lateral deformation of thorax

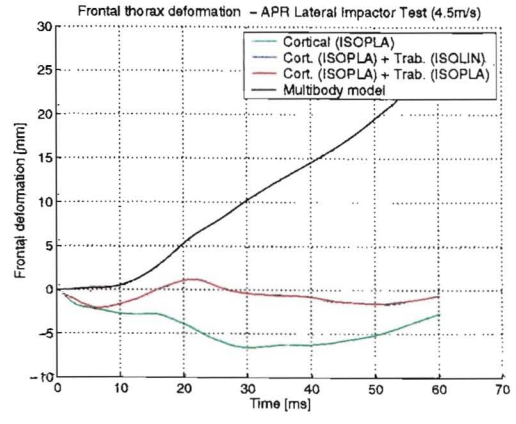

(e) Frontal deformation of thorax

Figure 7.7: Comparison of the response of the multibody and finite element models to the ISO pendulum impact.

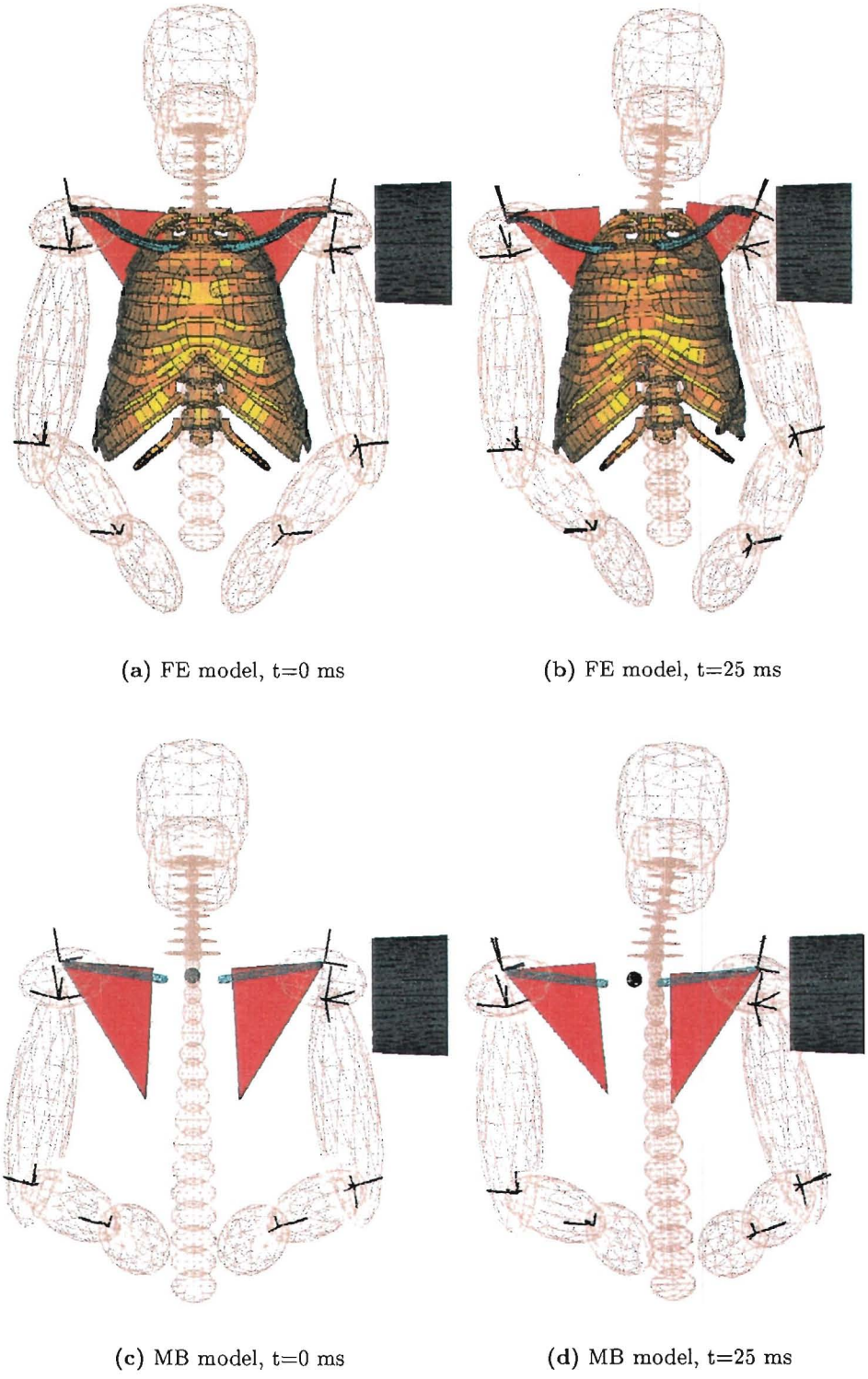

(a) FE model, t=0 ms

(b) FE model, t=25 ms

(c) MB model, t=0 ms

(d) MB model, t=25 ms

Figure 7.8: Frontal view of the finite element shoulder/thorax model and the multibody model during the ISO pendulum impact

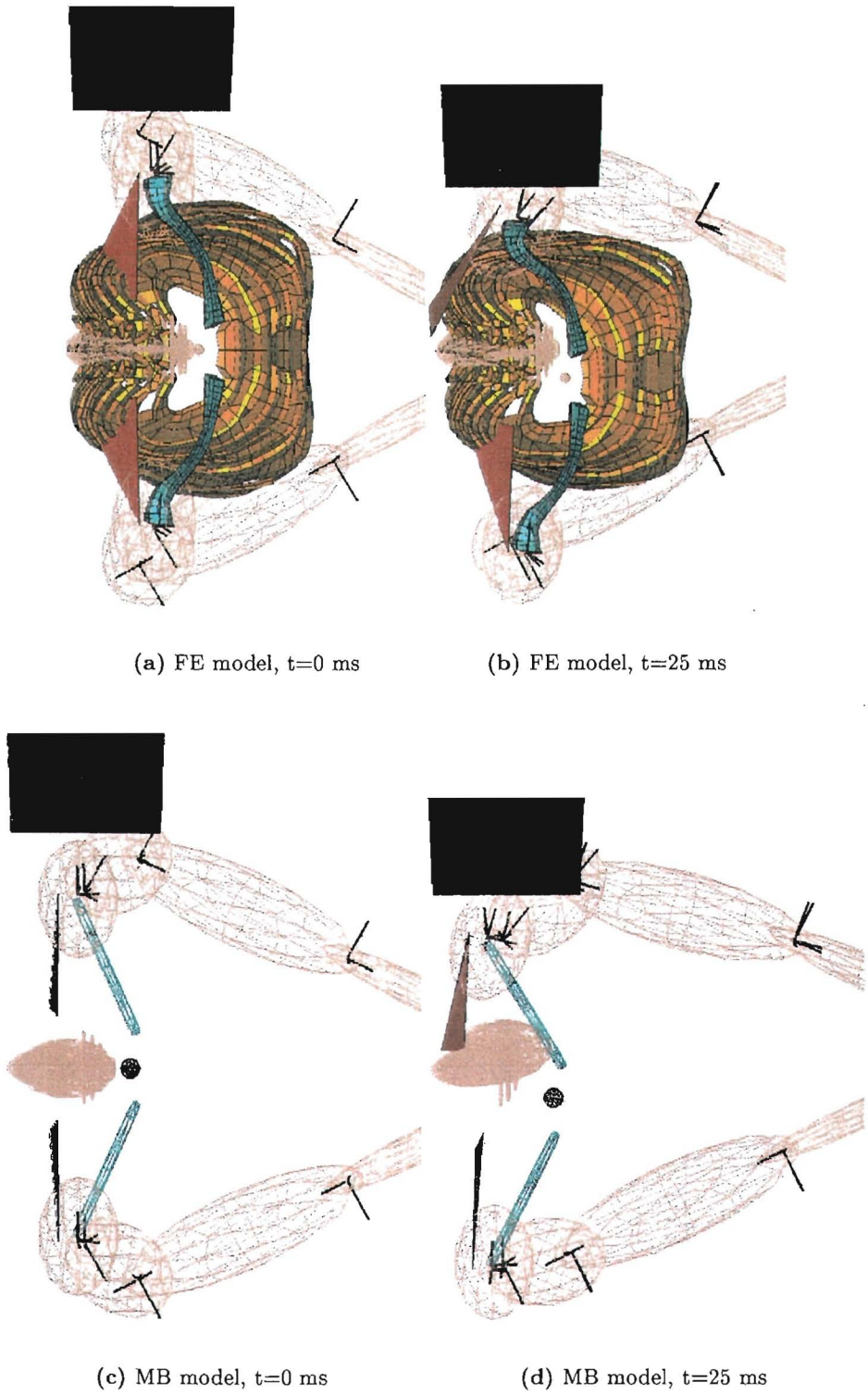

(a) FE model, t=0 ms (b) FE model, t=25 ms

(c) MB model, t=0 ms (d) MB model, t=25 ms

Figure 7.9: Top view of the finite element shoulder/thorax model and the multibody model during the ISO pendulum impact

Chapter 8

Discussion

The main objective of this study was the development of a design and research tool to evaluate injury risk to the shoulder girdle and upper extremity. Literature study showed that existing shoulder models were mainly lacking a biofidelic input resulting in poor validation results, and hence poor injury prediction capabilities. Therefore, it was decided to develop improved shoulder and arm models. The behavior and applicability of two types of shoulder models and a multibody arm model is discussed in this chapter:

Multibody shoulder model

The multibody shoulder model presented in this report shows good validation results with respect to available response requirements. It has to be noticed that these response requirements are based on a limited amount of cadaver experiments. The model is capable of predicting the load transfer from shoulder to spine through different loadpaths and it predicts well deformations occurring in the shoulder girdle. Injury prediction capabilities have to be defined with the use of global entities like displacements, accelerations, forces and moments. Most severe injuries during collisions are fracture of clavicle and/or scapula, and dislocations of the glenohumeral and/or acromioclavicular articulations:

- Clavicle fractures during lateral impact can be related to the maximum force occurring in the clavicle-sternum translational force model. Axial compression experiments on clavicles are available to derive injury tolerances.
- Clavicle fractures as a result of severe shoulder belt loading can be related to maximum moments in the clavicle. Three-point bending experiments on clavicles are available to derive injury tolerances.
- Acromioclavicular (AC) dislocations are a result of rupture of the acromioclavicular and/or coracoclavicular ligaments. These structures are not separately modeled, but characteristics are lumped in a rotational force model, which restraints the rotations of the AC joint. Maybe, joint injuries can be related to a maximum angle or maximum moment occurring in the AC rotational force model.

- Glenohumeral (GH) dislocations are mostly not a result of extreme rotational excursions of the arm, but a result of relative displacement of the humerus head with respect to the glenoid fossa. This movement is not allowed in the current model. Though, the direction of the resulting force in the joint may be a measure for injury.

Finite element shoulder model

A validated finite element clavicle model has been successfully integrated with a finite element thorax model and a multibody human model. The first evaluations showed promising results. The finite element approach allows the prediction of local fractures with the use of entities like stress and strain. However, it has to be noticed that, since a biofidelic thickness of the cortical bone is not available, an uniform thickness of the elements is adjusted to provide a good match to the results of the quasi-static three point bending experiments. This approach has the major disadvantage that, despite of the fact that global deformations can be predicted well, conclusions about local strains and stresses are difficult.

The major advantage of this model compared to the multibody shoulder model is the realistic integration of the shoulder model with a validated thorax model. Especially, inertial and visco-elastic effects, which are not present in the multibody shoulder model, contribute to a more realistic shoulder-thorax interaction. The FE model gives an understanding of the distribution of total shoulder deformation over the different segments, i.e. clavicle, thorax and joints.

Multibody arm model

Few validation data are available to perform simple, kinematical evaluations. Research has mainly focused on fracture mechanisms and tolerances. Most severe injuries during lateral collisions and airbag deployments are fracture of humerus, radius and ulna, and injury to the elbow and wrist:

- Since bending loads are assumed to be the main cause of humerus fractures, these fractures can be related to maximum moments in the humerus. Note that established injury tolerances for humerus fracture define different tolerances for the anterio-posterior and the lateral-medial direction.
- Bending loads are also the main cause of radius and ulna fractures. Most important to notice is that injury tolerances of the lower arm are dependent on the position of the lower arm (supinated or pronated).
- Elbow and wrist injuries as a result of airbag deployments are a current subject of research. Probably, elbow injuries are related to injury to the cartilage in the joint and to fractures of the distal humerus and proximal radius and ulna. Injury potential can be related to axial loads in the long bones, but is strongly dependent on the position of the joint. Wrist injuries consist of dislocations and fractures of the carpal bones and may be related to a combination of axial hand load and extreme joint rotations.

Chapter 9

Conclusions and recommendations

Within the scope of a study to develop numerical tools to predict injuries to the human body during impact conditions, an improved shoulder and upper extremity model based on multibody (MB) techniques is proposed. As a first step in the development of a complete finite element (FE) human body model, a validated FE clavicle model is integrated with Van der Made's FE thorax model [50] and TNO's MB human body model [20].

9.1 Conclusions

- The MB shoulder model shows acceptable kinematical response for the lateral impact direction. Due to a lack of experimental data no quantitative conclusions can be drawn about other directional responses. Compared to existing models, major improvements are achieved in the field of realistic input, biofidelic response and injury prediction capability.
- Two load paths from the shoulder to the spine can be distinguished. The major part of the load is transmitted through the clavicle connection; the other part is transmitted through the scapulo-thoracic connection. However, no experimental data are available to verify the correct ratio.
- Deformation characteristics of the clavicle are included and based on PMHS axial clavicle loading experiments. These experiments show no apparent strain-rate dependency and age dependency for clavicle bone.
- Evaluation of TNO's flexible body thorax model showed that a realistic coupling of the shoulder and thorax model is not possible. Though, deformation characteristics of the thorax are included in the shoulder model and are based on finite element simulations of Van der Made's thorax model.
- Three-point bending experiments and axial compression experiments on fresh clavicles are simulated with a FE clavicle model. Model responses were acceptable for

both loading conditions and therefore, this clavicle model should be able to predict frontal seatbelt loading and lateral impact loadings.

- This validated finite element clavicle model has been successfully integrated with the finite element thorax model of Van der Made and TNO's multibody human model. Comparison of this hybrid model and the multibody shoulder model showed that there is a need to implement a biofidelic coupling between the MB shoulder model and the MB thorax model. Due to the absence of correct inertial and visco-elastic effects, the force model that represents thorax deformation is too compliant.
- The multibody arm model presented is an extended version of the arm in the TNO human body model. The kinematical behavior is evaluated with a limited amount of free-swing experiments and PMHS pendulum impact. A general conclusion is that only a multibody approach is not sufficient as injury prediction and research tool.

9.2 Recommendations

Shoulder

The shoulder model shows to be promising, but major improvements can be obtained in the following areas:

- The MB shoulder model needs to be coupled to a MB thorax model in order to implement a biofidelic shoulder - thorax interaction.
- Frontal and vertical evaluations of the shoulder model are desirable in order to predict the interaction of the shoulder with seatbelts and airbags.
- More attention has to be given to the movement and function of the scapula. A virtual contact surface can be defined on which a facet surface description of the scapula (already available at TNO) slides.
- Injury prediction of joint dislocations requires more detailed modeling of structures that keep the joint intact (i.e. muscles and ligaments).

Arm

Major improvements in the modeling of the upper extremity can be obtained in the following areas:

- Available test data are to complicated to perform good validations of the multibody arm model. Therefore, more simple, kinematical experiments are necessary.
- Because of the difficulty to show unambiguous correlation between arm injury and multibody model output, the use of finite element techniques in the upper extremity is recommended. A great amount of experimental data are already available at the University of Heidelberg and Virginia.

Bibliography

[1] Centraal Bureau voor de Statistiek. http://neon.vb.cbs.nl/statweb/indexned.stm, 1999.

[2] A. Irwin, *Analysis and CAL3D model of the shoulder and thorax responses of seven cadavers subjected to lateral impacts.* PhD thesis, Wayne State University, 1994.

[3] E. Culham and M. Peat, "Functional anatomy of the shoulder complex," *Journal of Orthopaedic and Sports Physical Therapy*, vol. 18, no. 1, pp. 342–350, 1993.

[4] M. Peat, "Functional anatomy of the shoulder complex," *Physical therapy*, vol. 66, no. 12, pp. 1855–1865, 1986.

[5] E. Flatow, "The biomechanics of the acromioclavicular, sternoclavicular and scapulothoracic joints," *Instructional Course Lectures*, pp. 337–245, 1993.

[6] R. Happee, P. Morsink, and J. Wismans, "Mathematical human body modelling for impact loading," in *Proceedings of the SAE International Conference and Exposition on Digital human modelling for design and engineering*, no. 01-1909, Society of Automotive Engineers, 1999.

[7] F.C.T. van der Helm, *The shoulder mechanism: a dynamic approach.* PhD thesis, Delft University of Technology, 1991.

[8] S. Duma, *Injury criteria for the small female upper extremity.* PhD thesis, University of Virginia, 2000 (To be published).

[9] A. Engin, "On the biomechanics of the shoulder complex," *Journal of Biomechanics*, vol. 13, pp. 575–590, 1980.

[10] Z. Dvir and N. Berne, "The shoulder complex in elevation of the arm: A mechanism approach," *Journal of biomechanics*, vol. 11, no. 5, pp. 219–255, 1978.

[11] C. Högfors, B. Peterson, G. Sigholm, and P. Herberts, "Biomechanical model of the human shoulder joint: II: The shoulder rhythm," *Journal of Biomechanics*, vol. 24, no. 8, pp. 699–709, 1991.

[12] C. Högfors, D. Karlsson, and B. Peterson, "Structure and internal consistency of a shoulder model," *Journal of Biomechanics*, vol. 28, no. 7, pp. 767–777, 1995.

[13] A. Engin and S. Chen, "Statistical database for the biomechanical properties of the human shoulder complex - I: Kinematics of the shoulder complex," *Journal of Biomechanical Engineering*, vol. 108, no. 3, pp. 215–221, 1986.

[14] A. Engin and S. Chen, "Statistical database for the biomechanical properties of the human shoulder complex - II: Passive resistive properties beyond the shoulder complex sinus," *Journal of Biomechanical Engineering*, vol. 108, no. 3, pp. 222–227, 1986.

[15] A. Engin and S. Chen, "A statistical investigation of the *in vivo* biomechanical properties of the human shoulder complex," *Mathl. Comput. Modelling*, vol. 12, no. 12, pp. 1569–1582, 1989.

[16] A. Engin and S. Tümer, "Three-dimensional kinematic modelling of the human shoulder complex - part I: Physical model and determination of joint sinus cones," *Journal of Biomechanical Engineering*, vol. 111, pp. 107–112, 1989.

[17] S. Tümer and A. Engin, "Three-dimensional kinematic modelling of the human shoulder complex - part II: Mathematical modelling and solution via optimization," *Journal of Biomechanical Engineering*, vol. 111, pp. 113–121, 1989.

[18] X. Wang, F. Mazet, M. Maurin, N. De Castro Maia, K. Voinot, J. Verriest, and M. Fayet, "Three-dimensional modelling of the motion range of axial rotation of the upper arm," *Journal of Biomechanics*, vol. 31, pp. 899–908, 1998.

[19] W. Dempster, "Mechanisms of shoulder movement," *Archives of Physical Medicine & Rehabilitation*, vol. 46, no. 1-A, pp. 49–69, 1965.

[20] R. Happee, M. Hoofman, v. d. A. Kroonenberg, P. Morsink, and J. Wismans, "A mathematical human body model for frontal and rearward seated automotive impact loading," *SAE Paper*, vol. 983150, 1998.

[21] I. Kapandji, *The physiology of the joints*, vol. 3 - The trunk and vertebral column. Edinburgh, London and New York: Churchill Livingstone, 1974.

[22] A. Engin, R. Peindl, N. Berme, and I. Kaleps, "Kinematic and force data collection in biomechanics by means of sonic emitters," *Journal of Biomechanical Engineering*, vol. 106, no. 3, pp. 204–219, 1984.

[23] A. Engin and R. Peindl, "On the biomechanics of human shoulder complex - I: Kinematics for determination of the shoulder complex sinus," *Journal of Biomechanics*, vol. 20, no. 2, pp. 103–117, 1987.

[24] R. Peindl and A. Engin, "On the biomechanics of human shoulder complex - ii: Passive resistive properties beyond the shoulder complex sinus," *Journal of Biomechanics*, vol. 20, no. 2, pp. 119–134, 1987.

[25] A. Engin, "On the damping properties of the shoulder complex," *Journal of Biomechanical Engineering*, vol. 106, no. 11, pp. 360–363, 1984.

[26] H. Mertz, "A procedure for normalizing impact response data," *SAE Paper*, vol. 840884, 1984.

[27] F. Bendjellal, G. Walfish, A. Fayon, and C. Tarriere, *APR Biomechanical data.* Nanterre France, 1984.

[28] ISO-WG5, *Road vehicles - Anthropomorphic side impact dummy - Lateral response requirements to assess the biofidelity of the dummy*, ISO/TC22/SC12/WG5 - Document N455 - Revision 4 ed., 1997.

[29] J. Cavanaugh, T. Walilko, A. Malhotra, Y. Zhu, and A. King, "Biomechanical response and injury tolerance of the thorax in twelve sled side impacts," *SAE Paper*, vol. 902307, 1990.

[30] A. Irwin, T. Walilko, J. Cavanaugh, Y. Zhu, and A. King, "Displacement responses of the shoulder and thorax in lateral sled impacts," *SAE Paper*, vol. 933124, 1993.

[31] M. Maltese, *NHTSA Sled test data (*not yet available*).* National Highway Traffic Safety Administration, 2000.

[32] P. Palaniappan Jr., P. Wipasuramonton, P. Begeman, A. Tanavde, and F. Zhu, "A three-dimensional finite element model of the human arm," *SAE Paper*, vol. 99SC25, pp. 351–361, 1999.

[33] D. Kallieris, A. Rizetti, R. Mattern, S. Jost, P. Priemer, and M. Unger, "Response and vulnerability of the upper arm through side air bag deployment," *SAE Paper*, vol. 973323, 1997.

[34] S. Duma, B. Schreiber, J. McMaster, J. Crandall, C. Bass, and W. Pilkey, "Dynamic injury tolerances for long bones of the female upper extremity," in *Proceedings of IRCOBI Conference '98 - Goteborg*, pp. 189–201, 1998.

[35] S. Duma, J. Crandall, S. Hurwitz, and W. Pilkey, "Small female upper extremity interaction with a deploying side airbag," *SAE Paper*, vol. 983148, pp. 47–63, 1998.

[36] C. Bass, S. Duma, J. Crandall, R. Morris, P. Martin, W. Pilkey, S. Hurwitz, N. Khaewpong, R. Eppinger, and E. Sun, "The interaction of air bags with upper extremities," *SAE Paper*, vol. 973324, 1997.

[37] D. Huelke, R. Gilbert, and L. Schneider, "Upper-extremity injuries from steering wheel airbag deployments," *SAE Paper*, vol. 970493, 1997.

[38] W. Hardy, L. Schneider, M. Reed, and L. Ricci, "Biomechanical investigation of airbag-induced upper extrimity injuries," *SAE Paper 973325*, vol. 973325, pp. 131–137, 1997.

[39] Y. Huang, A. King, and J. Cavanaugh, "A MADYMO model of near-side human occupants in side impacts," *SAE Paper*, vol. 942207, 1994.

[40] Y. Huang, A. King, and J. Cavanaugh, "Finite element modeling of gross motion of human cadavers in side impact," *Journal of Biomechanical Engineering*, vol. 116, no. 5, pp. 228–235, 1994.

[41] E. Lizee, S. Robin, E. Song, N. Bertholon, J. Le Coz, B. Besnault, and F. Lavaste, "Development of a 3D finite element model of the human body," *SAE Paper*, vol. 983152, 1998.

[42] E. Meyer and J. Bonnoit, "Le choc lateral sur l'epaule: mise en place d'un protocole experimental en sollicitation dynamique," memoire de dea, Laboratoire de biomechanique appliquee, Faculte de Marseille, 1994.

[43] R. Jost and G. Nurick, "Finite element modelling of the human body in vehicle side impact," *IJCrash*, vol. 4, no. 1, pp. 31–37, 1999.

[44] G. Plank, M. Kleinberger, and R. Eppinger, "Fe modeling and analysis of thorax/restraint system interaction," in *Proceedings of 14th ESV Conference*, pp. 210–219, 1994.

[45] M. Iwamoto, K. Miki, B. Sambamoorthy, K. Yang, and A. King, "Development of finite element model of the human shoulder," in *Proceedings of Wayne State University's 60th Anniversary Symposium on Impact Biomechanics*, pp. 55–62, Wayne State University, 1999.

[46] E. Haug, M. Beaugonin, A. Tramecon, and L. Hyncik, "Current status of articulated and deformable human models for impact and occupant safety simulation at ESI group," in *Proceedings of PAM'98 User's Conference - Tours(France)*, Engineering Systems International, 1998.

[47] E. van Hassel, "Modelling of the human shoulder complex in impact conditions," WFW-report 98.024, Eindhoven University of Technology, 1998.

[48] J. Pelletiere, "Computational strength determination of human long bones," *SAE Paper*, vol. 1999-01-1904, pp. 1–10, 1999.

[49] P. Morsink, R. Happee, H. Cappon, and R. de Lange, "Madymo mathematical human body modeling; a 50th percentile male model," tno report 99.or.bv.025.1/pm, TNO Automotive, Delft, 1999.

[50] R. van der Made, "Development of a human thorax model (using finite element techniques in madymo)," WFW-report 2000.08, Eindhoven University of Technology, 2000.

[51] L. Obergefell and I. Kaleps, "Program for the generation of human body properties," in *Proceedings of Third International MADYMO Users' Meeting*, pp. 9–17, 1992.

[52] A. Engin and S. Chen, "Kinematic and passive resistive properties of human elbow complex," *Journal of Biomechanical Engineering*, vol. 109, pp. 318–323, 1987.

[53] S. Moroney, A. Schultz, J. Miller, and G. Andersson, "Load-displacement properties of lower cervical spine motion segments," *Journal of Biomechanics*, vol. 21, no. 9, pp. 769–779, 1988.

[54] M. d. Jager, *Mathematical head-neck models for acceleration impact.* PhD thesis, Eindhoven, University of Technology, 1996.

[55] HUMOS Project, *HUMOS Mid Term Assessment Report - Confidential*, 7ERE/990517/P1/DA2 ed., 1999.

[56] G. Granik and I. Stein, "Human ribs: Static testing as a promising medical application," *Journal of Biomechanics*, vol. 6, pp. 237–240, 1973.

[57] V. Mow and W. Hayes, *Basic orthopaedic biomechanics.* Raven Press, New York, 1991.

[58] B. van Rietbergen, *Mechanical behavior and adaptation of trabecular bone in relation to bone morphology.* PhD thesis, University of Nijmegen, 1996.

Appendix A

Anatomical terminology

In the 'anatomical position' the body is erect, facing forward, arms stretched at the sides, and the palms facing forward. All definitions or descriptions of location, position or motion refer to this starting position.

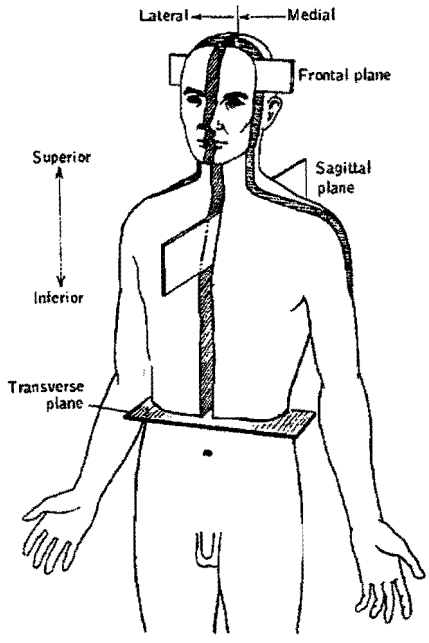

Principal planes :

Median plane	: The plane through the longitudinal axis and the sagittal axis, which divides the body in the right and left half
Sagittal plane	: Any plane which is parallel to the median plane
Frontal plane	: Any plane which contains transverse axes and is parallel to the forehead and perpendicular to the sagittal plane
Transverse plane	: plane perpendicular to the sagittal and frontal plane, dividing the body in upper and lower portions

Principal axes :

Longitudinal axis	: Vertical axis
Transverse axis	: Horizontal axis from left to right
Sagittal (or antero-posterior) axis	: Axis from front to back, perpendicular to the longitudinal and transverse axis

Anatomical directions :

Anterior	: toward the front
Posterior	: toward the rear
Inferior	: downward
Superior	: upward
Lateral	: away from the median plane
Medial	: toward the median plane
Dorsal	: toward the rear
Ventral	: toward the front/abdomen
Proximal	: toward the point of attachment of the limb
Distal	: farther away from the trunk

Directions of movement :

Flexion	: bending
Extension	: stretching
Abduction	: movement away from the median plane
Adduction	: movement towards the median plane
Depression	: downward movement
Elevation	: upward movement
Retraction	: backward movement
supination	: lateral rotation of the fore-arm
Pronation	: medial rotation of the fore-arm

Appendix B

Input of multibody model

The reference orientation and position of the models are shown in Figure B. No correction is made in the coordinate systems on opposite sides: Abduction of the left arm is defined by a positive rotation around the X-axis of the left shoulder joint. Abduction of the right arm is defined by a negative rotation around the X-axis of the right shoulder joint. This appendix presents the stiffness functions which are implemented in the force models as described in Chapter 5, and gives the exact motion ranges of the joints in the shoulder and arm model.

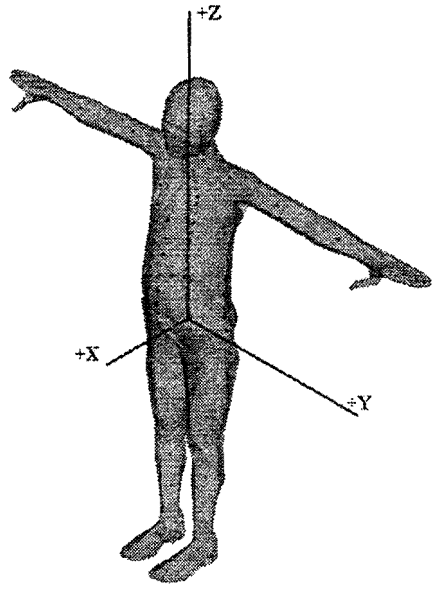

Figure B.1: Human model reference position and reference coordinate axis.

Functions in point-restraints

Clavicle - Sternum:
X-direction: -1.0m -3.0e5N , 1.0m 3.0e5N
Y-direction: -1.0m -3.0e5N , 1.0m 3.0e5N
Z-direction: -1.0m -1.5e6N , 1.0m 1.5e6N

Sternum - Vertebra T3:
X-direction: -1.0m -1.2e5N , 1.0m 1.2e5N
Y-direction: -1.0m -1.2e5N , 1.0m 1.2e5N
Z-direction: -1.0m -0.8e5N , 1.0m 0.8e5N

Scapula - Vertebra T3/T7:
X-direction: -0.05m -1.0e3N , -0.03m -2.0e2N , 0.0m 0.0N , 0.03m 2.0e2N , 0.05m 1.0e3N
Y-direction: -1.0m 0.0N , -1.0m 0.0N
Z-direction: -0.02m -1.0e2N , -0.01m -2.0e1N , 0.0m 0.0N , 0.05m 2.0e0N , 0.10m 1.0e1N

Functions in cardan-restraints

Sternoclavicular joint:
Right
X-rotation: down(+)/up(-), Range of motion $-15 < x < 25$ degrees
Y-rotation: back(-)/front(+), Range of motion $-5 < y < 15$ degrees
Z-rotation: front(+)/back(-), Range of motion $-15 < z < 35$ degrees
Left
X-rotation: down(-)/up(+), Range of motion $-25 < x < 15$ degrees
Y-rotation: back(+)/front(-), Range of motion $-5 < y < 15$ degrees
Z-rotation: front(-)/back(+), Range of motion $-35 < z < 15$ degrees

Acromioclavicular joint:
Right
X-rotation: down(+)/up(-), Range of motion $-15 < x < 15$ degrees
Y-rotation: back(-)/front(+), Range of motion $-15 < y < 15$ degrees
Z-rotation: front(+)/back(-), Range of motion $-20 < z < 20$ degrees
Left
X-rotation: down(-)/up(+), Range of motion $-15 < x < 15$ degrees
Y-rotation: back(+)/front(-), Range of motion $-15 < y < 15$ degrees
Z-rotation: front(+)/back(-), Range of motion $-20 < z < 20$ degrees

Glenohumeral joint:
Right
X-rotation: adduction(+)/abduction(-), Range of motion $-50 < x < 90$ degrees
Y-rotation: back(-)/front(+), Range of motion $-65 < y < 65$ degrees

Z-rotation: front(+)/back(-), Range of motion $-50 < z < 100$ degrees
Left
X-rotation: adduction(-)/abduction(+), Range of motion $-90 < x < 50$ degrees
Y-rotation: back(+)/front(-), Range of motion $-65 < y < 65$ degrees
Z-rotation: front(-)/back(+), Range of motion $-100 < z < 50$ degrees

Elbow joint:
Right
X-rotation: down(+)/up(-), Range of motion 0 degrees
Y-rotation: supination(+)/pronation(-), Range of motion $-90 < y < 90$ degrees
Z-rotation: flexion(+)/extension(-), Range of motion $-90 < z < 55$ degrees
Left
X-rotation: down(-)/up(+), Range of motion 0 degrees
Y-rotation: supination(-)/pronation(+), Range of motion $-90 < y < 90$ degrees
Z-rotation: flexion(-)/extension(+), Range of motion $-55 < z < 90$ degrees

Wrist joint:
Right
X-rotation: down(+)/up(-), Range of motion $-80 < x < 80$ degrees
Y-rotation: back(-)/front(+), Range of motion 0 degrees
Z-rotation: front(+)/back(-), Range of motion $-30 < z < 30$ degrees
Left
X-rotation: down(-)/up(+), Range of motion $-80 < x < 80$ degrees
Y-rotation: back(+)/front(-), Range of motion 0 degrees
Z-rotation: front(-)/back(+), Range of motion $-30 < z < 30$ degrees

Appendix C

Successive shoulder rotations

In the human body a rotation of the arm is a combined and simultaneous rotation in the glenohumeral, acromioclavicular and sternoclavicular articulations. In the shoulder model rotation of the arm is a successive rotation of the separate joints. These successive rotations are visualized in Figure C

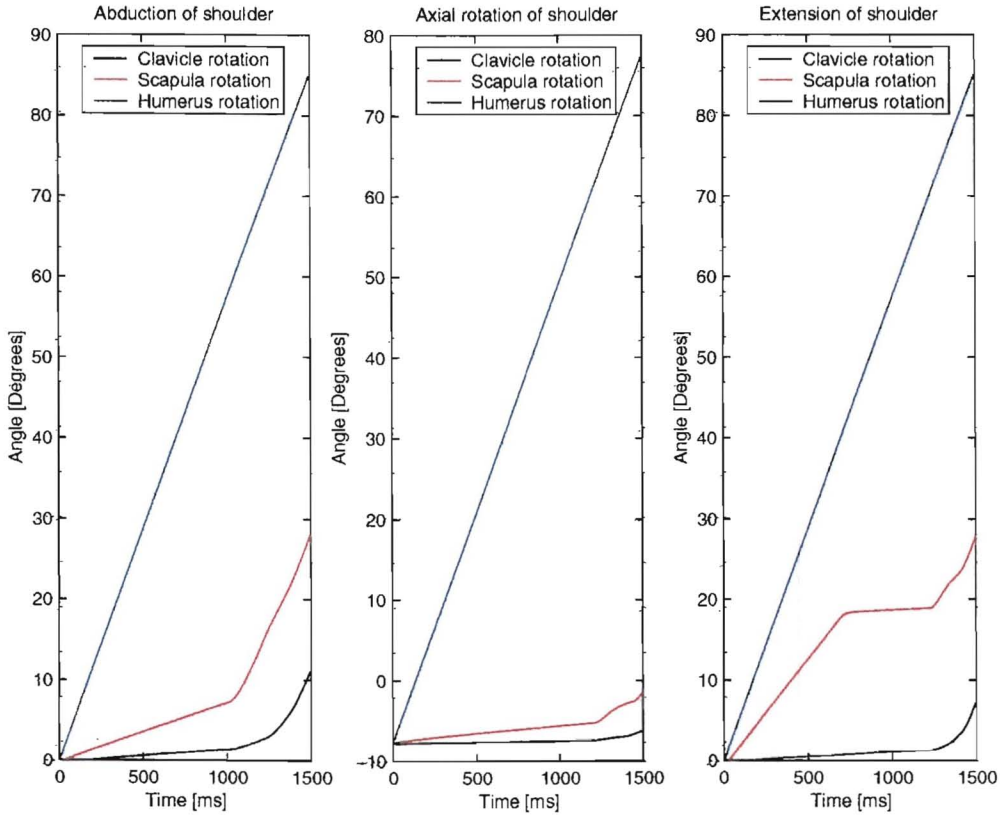

Figure C.1: Angle - Time relation of the multibody shoulder model for rotations about the principal axes.

Appendix D

Anthropometric data of cadavers

The table lists the anthropometric data of the cadavers used in the clavicle mechanical experiments performed at the University of Heidelberg.

Experiment no.	**Sex**	**Age** [years]	**Height** [cm]	**Weight** [kg]
55+56	M	37	176	61
57+58	M	49	175	84
85	M	31	180	67
86	M	32	180	54
87	M	27	180	77
94+98	M	30	179	84
95+99	M	58	180	101
96+100	M	63	172	71
97+101	M	55	176	92
103	M	58	180	101
104+110	M	22	176	70
105+111	M	33	178	88
106+112	M	51	179	82
107+113	M	39	171	77
108+114	M	34	193	95
109+115	M	37	184	77
149+150	M	34	177	88
157	M	50	173	67
158+159	M	28	170	65
160+161	M	54	184	104